



**University of
Zurich**^{UZH}

**Zurich Open Repository and
Archive**

University of Zurich
University Library
Strickhofstrasse 39
CH-8057 Zurich
www.zora.uzh.ch

Year: 2012

Polythiophenes inhibit prion propagation by stabilizing PrP aggregates

Margalith, Ilan ; Suter, Carlo ; Ballmer, Boris ; Schwarz, Petra ; Tiberi, Cinzia ; Sonati, Tiziana ; Falsig, Jeppe ; Nystrom, Sofie ; Hammarstrom, Per ; Aslund, Andreas ; Nilsson, K Peter R ; Yam, Alice ; Whitters, Eric ; Hornemann, Simone ; Aguzzi, Adriano

Abstract: LCPs interact with ordered protein aggregates and sensitively detect amyloids of many different proteins, suggesting that they may possess antiprion properties. Here we show that a variety of anionic, cationic and zwitterionic LCPs reduced the infectivity of prion-containing brain homogenates and of prion-infected cerebellar organotypic cultured slices COCS, and decreased the amount of PrP(Sc) oligomers that could be captured in an avidity assay. Paradoxically, treatment enhanced the resistance of PrP(Sc) to proteolysis, and triggered the compaction and enhanced the resistance to proteolysis of recombinant mPrP(23-231) fibers. These results suggest that LCPs act as antiprion agents by transitioning PrP aggregates into structures with reduced frangibility. Moreover, ELISA on COCS and in vitro conversion assays with mPrP(23-231) indicated that PTAA may additionally interfere with the generation of PrP(Sc) by stabilizing the conformation of PrP(C) or of a transition intermediate. Therefore, LCPs represent a novel class of antiprion agents whose mode of action appears to rely on hyperstabilization, rather than destabilization, of PrP(Sc) deposits.

DOI: <https://doi.org/10.1074/jbc.M112.355958>

Posted at the Zurich Open Repository and Archive, University of Zurich

ZORA URL: <https://doi.org/10.5167/uzh-61798>

Journal Article

Accepted Version

Originally published at:

Margalith, Ilan; Suter, Carlo; Ballmer, Boris; Schwarz, Petra; Tiberi, Cinzia; Sonati, Tiziana; Falsig, Jeppe; Nystrom, Sofie; Hammarstrom, Per; Aslund, Andreas; Nilsson, K Peter R; Yam, Alice; Whitters, Eric; Hornemann, Simone; Aguzzi, Adriano (2012). Polythiophenes inhibit prion propagation by stabilizing PrP aggregates. *Journal of Biological Chemistry*, 287(23):18872-18887.

DOI: <https://doi.org/10.1074/jbc.M112.355958>

Polythiophenes inhibit prion propagation by stabilizing PrP aggregates*

Ilan Margalith¹, Carlo Suter¹, Boris Ballmer¹, Petra Schwarz¹, Cinzia Tiberi¹, Tiziana Sonati¹, Jeppe Falsig¹, Sofie Nyström², Per Hammarström², Andreas Åslund², K. Peter R. Nilsson², Alice Yam³, Eric Whitters³, Simone Hornemann¹ and Adriano Aguzzi¹

¹ Institute of Neuropathology, University Hospital of Zurich, CH-8091 Zurich, Switzerland

² Department of Chemistry, University of Linköping, Sweden

³ Novartis Diagnostics, 4560 Horton Street, Emeryville, CA 94608, USA

*Running title: *Luminescent conjugated polymers as antiprion compounds*

To whom correspondence may be addressed: Adriano Aguzzi and Simone Hornemann, University Hospital of Zürich, Institute of Neuropathology, Schmelzbergstrasse 12, CH-8091 Zurich, Switzerland, Tel.: +41 44 255 21 07, Fax number: +41 44 255 44 02, Email: Adriano.Aguzzi@usz.ch and Simone.Hornemann@usz.ch

Keywords: therapy; antiprion activity; luminescent conjugated polymers; transmissible spongiform encephalopathies; prion diseases

Background: Luminescent conjugated polymers (LCPs) are highly specific to amyloid conformations and may represent potential antiprion compounds.

Results: LCPs significantly reduce prion titers, while rendering PrP^{Sc} more stable to proteolytic digestion.

Conclusion: LCPs possess pronounced antiprion potential and appear to act by compaction of frangible fibers.

Significance: LCPs may represent novel pharmacophores for the prevention and treatment of prion diseases.

SUMMARY

LCPs interact with ordered protein aggregates and sensitively detect amyloids of many different proteins, suggesting that they may possess antiprion properties. Here we show that a variety of anionic, cationic and zwitterionic LCPs reduced the infectivity of prion-containing brain homogenates and of prion-infected cerebellar organotypic cultured slices (COCS), and decreased the amount of PrP^{Sc} oligomers that could be captured in an avidity assay. Paradoxically, treatment enhanced the resistance of PrP^{Sc} to proteolysis, and triggered the compaction and enhanced the resistance to proteolysis of recombinant mPrP₂₃₋₂₃₁ fibers. These results suggest that LCPs act as antiprion agents by transitioning PrP aggregates into structures with reduced frangibility. Moreover, ELISA on COCS and

in vitro conversion assays with mPrP₂₃₋₂₃₁ indicated that PTAA may additionally interfere with the generation of PrP^{Sc} by stabilizing the conformation of PrP^C or of a transition intermediate. Therefore, LCPs represent a novel class of antiprion agents whose mode of action appears to rely on hyperstabilization, rather than destabilization, of PrP^{Sc} deposits.

Prion diseases are neurodegenerative, infectious disorders characterized by the deposition of β -sheet rich aggregates. These invariably fatal diseases can be inherited (1), arise spontaneously (2), or develop upon transmission of prion infectivity (3-5). The infectious agent is termed prion and is mainly composed of PrP^{Sc}, a partially protease-resistant isoform of the physiologically occurring prion protein PrP^C (6). PrP^{Sc} condenses into macromolecular aggregates that accumulate within the CNS and to a lesser extent in other organs (6,7). The conversion of PrP^C into PrP^{Sc} can be triggered by transmitting prions between organisms. Also, it is becoming increasingly evidence that many amyloid diseases progress through the trans-cellular propagation of prion-like seeds termed "prionoids" (8,9).

No efficient treatments against prion diseases are available (10). The central role played by PrP^{Sc} in prion diseases has inspired searches for compounds influencing PrP^{Sc} stability and/or clearance. Inhibition of PrP^{Sc} conversion in prion-infected cultured cells (11) or in animal models (12) was reported for molecules that can cross the

blood-brain barrier (BBB) such as amphotericin B (12), quinacrine, and chlorpromazine. However, clinical trials in humans revealed no significant improvements of the course of chronic disease (13-15).

Several polyanions can interfere with prion replication. Congo red (CR) (16) and the fluorescent antracycline iododoxorubicin (17) prolong incubation time in rodents upon co-inoculation with prions. CR interacts with, and stabilizes, PrP^{Sc} (18), whereas iododoxorubicin binds to PrP^{Sc} deposits in brain sections of CJD patients (17). It is therefore likely that the interaction of such compounds with infectious prion species is responsible for a decrease of prion infectivity. Therefore, compounds that stabilize prions could represent valuable tools for the treatment or the prophylaxis of prion diseases.

The structural requirements for the antiprion activity of sulphated polyanions in chronically infected cells were investigated in detail (19). These compounds are believed to interfere with the interaction of endogenous glycosaminoglycans with PrP^C and/or PrP^{Sc} rather than acting directly onto PrP^{Sc} aggregates. The most promising compound, pentosan polysulfate (PPS) (20,21) is currently undergoing clinical trials despite its poor pharmacokinetics and high toxicity (22). Finally, complex polyamines have been shown to disaggregate PrP but suffer poor bioavailability (23). Therefore it would be desirable to identify new classes of compounds with drug-like properties (including high bioavailability and low toxicity) that directly influence amyloid propagation.

Luminescent conjugated polythiophenes (LCPs) are versatile probes with striking affinity to variety of amyloids (24-27). Upon binding amyloids, LCPs adopt distinct conformations with characteristic spectral properties (28) specific to distinct amyloid types (27). Newer-generation LCPs efficiently cross the blood-brain barrier, enabling visualization of protein aggregates in vivo and, potentially, clinical trials.

Here we investigate the potential of various LCPs as novel antiprion compounds. All tested LCPs significantly reduced prion infectivity while increasing the protease resistance of PrP^{Sc}. We therefore posit that the polythiophene scaffold is a novel, generic amyloid-stabilizing pharmacophore which could spawn useful antiprion compounds.

EXPERIMENTAL PROCEDURE

General methods of the synthesis of PBAT – Organic extracts were dried over anhydrous magnesium sulfate, filtered and concentrated *in vacuo* at 40 °C. All chemicals were purchased from Sigma-Aldrich Co (Sigma-Aldrich, St. Louis, MO, USA) and used as is. NMR spectra were recorded on a Varian 80 instrument (¹H 300 MHz, ¹³C 75.4 MHz, Varian Inc., Santa Clara, CA, USA). Chemical shifts were assigned with the solvent residual peak as a reference according to Gottlieb *et al.* (76). Thin layer chromatography (TLC) was carried out on Merck precoated 60 F254 plates (Merck, Whitehouse Station, NJ, USA) 85 using UV light (λ = 254 nm and 366 nm) and charring with ethanol/sulfuric acid/*p*-anisaldehyde/acetic acid 90:3:2:1 for visualization. Flash column chromatography (FC) was performed using silica gel 60 (0.040–0.063 mm, Merck). Gradient HPLC-MS was performed on a Gilson system (Gilson, Middleton, WY, 90 USA). Column: Waters X-Bridge C-18 5 μ m, 250 x 15 mm and Waters X-Bridge C-18 2.5 μ m, 150 x 4.6 mm for semipreparative and analytical runs respectively; using acetonitrile with 0.05% formic acid and deionized water with 0.05% formic acid as mobile phase. MALDI-TOFMS was recorded in linear positive mode with the analyte as matrix. Normal work up means that the organic extracts were dried on MgSO₄, filtered and concentrated *in vacuo*.

Synthesis of 2-(3-thienyl)-p-toluenesulfonyl ethanol (2) – 2-(Thiophene-3-yl) ethanol (0.700 g, 5.43 mmol) was added to a solution of CHCl₃ and pyridine (1:1, 12.0 ml). *p*-toluenesulfonyl chloride (1.24 g, 6.50 mmol) was added. After 16 h reaction was quenched by adding water (20 ml) and ether (100 ml). The organic layer was washed with HCl (1 M aq, 4 x 25 ml) and water (3 x 25 ml) and subjected to normal workup. The product was purified by FC (toluene) to give (2) (1.47 g, 97 %) as pale yellow oil. TLC (toluene) R_f=0.09

¹H-NMR (CDCl₃) δ : 2.44 (s, 3H), 2.99 (t, 2H, *J*=6.9), 4.21 (t, 2H, *J*=6.9), 6.87 (dd, 1H, *J*=1.5, 5.1 Hz), 6.97 (m, 1H), 7.23 (dd, 1H, *J*=3.0, 5.1 Hz), 7.31 (d, 2H, *J*=8.4 Hz), 7.73 (d, 2H, *J*=8.4 Hz).

¹³C-NMR (CDCl₃) δ : 21.6, 29.8, 69.9, 122.1, 125.8, 127.8, 128.0, 129.8, 133.3, 135.9, 144.9.

Synthesis of (S)-3-[2-(3-thienyl)-ethoxy]-2-tert-butoxycarbonylamino-propionic acid (3) – (2) (1.23 g, 4.36 mmol) was dissolved in dry DMF

(45 mL), *N*-Boc-L-Ser-OH (1.79 g, 8.72 mmol) and K_2CO_3 (1.81 g, 13.1 mmol) were added to the solution. The mixture was heated to 45 °C and the reaction was quenched after 24 h by pouring the mixture over ice and HCl (2 M aq). The product was extracted with toluene (3 x 40 ml), which was subsequently washed with HCl (2 M aq, 2 x 25 ml) and NaCl (sat. aq, 3 x 50 ml), followed by normal workup. The syrup was purified by FC (toluene → toluene/ethyl acetate, 4:1) and gave the colorless syrup product (**3**) (0.879 g, 64 %). TLC (toluene/ethyl acetate, 4:1) R_f =0.1

1H -NMR ($CDCl_3$) δ : 1.43 (s, 9H), 2.86 (s, 1H), 2.98 (t, 2H, J =6.9), 3.84 (dd, 1H, J =3.5, 11.3 Hz), 3.85 (dd, 1H, J =3.8, 11.3 Hz), 4.42 (m, 3H), 5.51 (d, 1H, J =7.8 Hz), 6.95 (dd, 1H, J =1.5, 4.6 Hz), 7.03 (dd, 1H, J =1.5, 2.9 Hz), 7.25 (dd, 1H, J =2.9, 4.6 Hz)

^{13}C -NMR ($CDCl_3$) δ : 28.2, 29.4, 55.7, 63.3, 65.2, 80.2, 121.7, 125.7, 128.1, 137.5, 155.7, 170.7

Synthesis of (R)-1-carboxy-N,N,N-trimethyl-2-(2-(thiophen-3-yl)ethoxy)ethanaminium (4) – (3) (0.692 g, 2.10 mmol), $NaHCO_3$ (0.706 g, 8.41 mmol) and methyl iodide (2.09 ml, 33.6 mmol) were dissolved in dry DMF (35 ml). After three days the reaction was diluted with toluene (100 ml) and co-evaporated to give a yellow solid. The precipitate was dissolved in methanol (50 ml) and washed with heptane (2 x 30 ml). The mixture was concentrated and the product was purified by HPLC [ACN/ H_2O , 5:95 14 min; flow: 7 mL/min; wavelength: 210 nm; Mass: 257.12 (calculated and found)] to afford (**4**) (0.565 g, 70 %) as pale yellow crystals.

1H -NMR (Methanol- d_4) δ : 3.07 (t, 2H, J =6.6 Hz), 3.31 (s, 9H),

4.16 (dd, 1H, J =5.4, 13.5 Hz), 4.23 (dd, 1H, J =3.3, 13.5 Hz), 4.39 (dd, 1H, J =3.3, 5.4 Hz), 4.48 (dt, 1H, J =6.6, 10.8 Hz), 4.56 (dt, 1H, J =6.6, 10.8 Hz), 7.05 (dd, 1H, J =1.5, 4.8 Hz), 7.20 (dd, 1H, J =1.5, 2.7 Hz), 7.36 (dd, 1H, J =2.7, 4.8 Hz)

^{13}C -NMR (Methanol- d_4) δ : 30.2, 54.3, 59.4, 67.6, 76.1, 123.1, 126.9, 129.2, 139.0, 166.8

Synthesis of Poly-((R)-1-carboxy-N,N,N-trimethyl-2-(2-(thiophen-3-yl)ethoxy)ethanaminium) (5) – (4) (0.172 g, 0.666 mmol), $FeCl_3$ (0.486 g, 3.00 mmol) and tetrabutylammonium-trifluoromethanesulfonate (0.521 g, 1.33 mmol) was added to a solution of dry chloroform (13.5 ml). After 2 h the mixture was quenched by adding water (3 ml). The organic layer was extracted by water (2 x 3 ml).

The aqueous solution was made acidic by HCl (conc. aq) and acetone was added to the mixture until the polymer precipitated as red flakes. The mixture was centrifuged and the yellow water was decanted. The procedure was repeated until the yellow color, from dissolved $FeCl_3$, of the water had disappeared. The polymer was dissolved in water and lyophilized, resulting in a red powder (**5**) (0.0722 g, 37 % calculated with respect to the monomeric unit).

Preparation of LCP stock solutions – The synthesis of the other different LCPs has been described elsewhere (24,26,29-35,77). Lyophilized LCPs were resuspended in pure water (B. Braun, Melsungen AG) and stock solutions at a concentration of 1 mg ml^{-1} were prepared and stored at 4°C, protected from light. Serial dilutions of the LCPs were prepared in pure water.

Preparation of CD1 and RML6 crude brain homogenates and exposure to LCPs and PPS – 20% wt/vol CD1 or RML6 brain homogenates in 0.32 M sucrose in PBS were prepared by three runs in a Precellys24 tissue homogenizer (Bertin) with cooling on ice between each run. Protein concentrations of CD1 or RML6 brain homogenates were determined using the bicinchoninic acid assay (Pierce) and normalized to 1 mg ml^{-1} total protein with 0.32 M sucrose in PBS.

LCPs and PPS were diluted into aliquots of crude brain homogenates at final concentrations ranging from 10^{-4} to 5000 $\mu g\ ml^{-1}$ and to final volumes of 45 μl . All samples were incubated for 30 min at 37°C on a thermoshaker rotating at 700 rpm prior to proteolysis.

Treatment of slice cultures with LCPs – Cerebellar slice cultures were prepared and prion-infected according to a protocol described by Falsig et al. (43,44). Slice culture medium was changed three times per week and 10 μl of diluted PTAA or PPS (30 $\mu g\ ml^{-1}$, Bene pharmachem) was added to 1 ml medium to obtain final concentrations ranging from 0.01 to 60 $\mu g\ ml^{-1}$ PTAA or 0.3 $\mu g\ ml^{-1}$ PPS. Treatment was initiated three weeks post-infection or in a time-course manner and maintained until tissue was harvested. Tissue was harvested in PBS and homogenized according to a protocol described by Falsig et al. (43,44). Protein concentration was determined using the bicinchoninic acid assay (Pierce) and normalized to 1 mg ml^{-1} total protein with PBS.

Western blot analysis – PrP^{Sc} was detected by limited proteolysis with PK (Roche) and analysed by Western blotting. Samples of 45 µl brain homogenate or 20 µl aliquots from slice culture homogenates containing 20 µg protein were digested with 50 µg ml⁻¹ PK and 25 µg ml⁻¹ PK, respectively, in lysis buffer containing 0.5% wt/vol sodium deoxycholate, 0.5% vol/vol Nonidet P-40 and 10% vol/vol PBS for 60 min at 37°C and rotating at 700 rpm on a thermoshaker.

PK digestion was terminated by adding 17 µl of 4x LDS loading buffer (NuPAGE, Invitrogen) and boiling the samples at 95 °C for 5 min. 30 µl of the samples were separated on a 12% Bis-Tris SDS polyacrylamide gel (NuPAGE, Invitrogen) and blotted onto a nitrocellulose membrane. Membranes were blocked with 5% wt/vol Topblock (Fluka) in Tris-buffered saline supplemented with Tween (150 mM NaCl, 10 mM Tris HCl, 0.05% Tween 20 (vol/vol)) and incubated with POM1 mouse IgG1 antibody to PrP^C (anti-PrP^C) (200 ng ml⁻¹) as primary antibody. Horseradish peroxidase (HRP)-conjugated rabbit anti-mouse IgG1 (1:10,000, Zymed) was used as a secondary antibody. The blots were developed using SuperSignal West Pico chemiluminescent substrate (Pierce) and detected in a LAS3000 system (FUJI).

Scrapie Cell End-Point Assay – SCEPA was performed as described previously (36). Briefly, RML6 samples consisting of 1% brain homogenate containing various concentrations of LCPs were diluted 1 to 100 fold in cell culture medium to obtain a final dilution of 10⁻⁴. These samples were then serially diluted in cell culture medium containing a 10⁻⁴ dilution of CD1 brain homogenate and dilutions of RML ranging from 10⁻⁴ to 10⁻⁸ in 96-well plates. Each experimental run comprised four plates with the first plate containing a 10⁻⁴ to 10⁻⁸ decadal dilution of untreated RML6 as a control. The other three plates were used to analyze the titer of three dilutions of one LCP, or of three distinct LCPs.

For slice culture homogenates, samples normalized to 1 mg ml⁻¹ total protein were diluted 1 to 100 fold in cell culture medium to obtain a final dilution of 10⁻⁴. These samples were then serially diluted in cell culture medium containing a 10⁻⁴ dilution of CD1 brain homogenate and dilutions of homogenates from COCS ranging from 10⁻⁴ to 10⁻⁸ and tested in 96-well plates. Experimental runs comprised four plates

including a homogenate of COCS from six weeks-old prion-infected, non-treated tissue as a standard plate. The infection of N2a-PK1 cells and subsequent processing of the SCEPA were performed as previously described (36).

Misfolded protein assay – Samples of 10 µg total protein (brain homogenate prepared as 1% w/v in 0.32 M sucrose in PBS and normalized to 1 mg ml⁻¹) from LCP-treated RML6 or 5 µg total protein from slice culture homogenates were diluted 100 fold in TBSTT (50 mM Tris-HCl (pH 7.5)/137 mM NaCl/1% Tween 20/1% Triton X-100) and incubated for 10 min at 37 °C under permanent agitation (850 rpm). 100 µl was then subjected to precipitation using magnetic beads coupled to the peptoid PSR1 (37) for 1 h at 37 °C under permanent agitation (750 rpm). Beads were washed and trypsin digestion was performed (12.5 µg ml⁻¹ trypsin in TBST containing 5 mM CaCl₂) for 30 min at 37 °C under permanent agitation (750 rpm) and stopped with 2 mM PMSF for 15 min at RT. Beads were washed and denatured with 0.1 N NaOH. After neutralization (0.3 M Na₂H₂PO₄), samples were placed on a magnet, and the supernatant was transferred to POM19 (40)-coated ELISA plates. After incubation (1 h at 37°C, 300 rpm), plates were washed, and AP-conjugated POM2 (40) was added. After incubation with substrate (100 µl of Lumiphos Plus substrate (Lumigen, Southfield, MI), plates were read in a luminometry reader (Luminoskan Ascent; Thermo Fisher Scientific).

Bead-based capture of PrP^{Sc} – 21 µl of PSR1-conjugated beads (37) were washed five times in 1 ml PBS (8 mM Na₂HPO₄, 1.5 mM KH₂PO₄, 137 mM NaCl, 2.7 mM KCl, pH7.4) before incubation with different dilutions of a 10% RML6 brain homogenate ranging from 10⁻² to 10⁻¹⁰ overnight at 4°C upon shaking at 1000 rpm.

Unbound material was removed from the beads by washing five times with 1 ml of PBS. The beads were resuspended in 60 µl or 120 µl in PBS and 30 µl, respectively, of the resuspended beads were intracerebrally inoculated into tga20 mice with groups of at least 4 mice.

Mice were monitored every second day, and TSE was diagnosed according to clinical criteria including ataxia, wobbling, and hind leg paresis. At the onset of terminal disease tga20 mice were sacrificed. Mice were maintained under conventional conditions, and all experiments were

performed in accordance with the animal welfare guidelines of the Kanton of Zürich.

Histopathology and immunohistochemical stains – Two- μm thick sections were cut onto positively charged silanized glass slides and stained with hematoxylin and eosin, or immunostained using antibodies for PrP (SAF84), for astrocytes (GFAP). For PrP staining, sections were deparaffinized and incubated for 6 min in 98% formic acid, then washed in distilled water for 5 min.

Sections were heat-treated and immunohistochemically stained on an automated NEXES immunohistochemistry staining apparatus (Ventana Medical Systems, Switzerland) using an IVIEW DAB Detection Kit (Ventana). After incubation with protease 2 (Ventana) for 16 min, sections were incubated with anti-PrP SAF-84 (SPI bio; 1:200) for 32 min. Sections were counterstained with hematoxylin. GFAP immunohistochemistry for astrocytes (rabbit anti-mouse GFAP polyclonal antibody 1:1000 for 24 min; DAKO) was similarly performed, however with antigen retrieval by heating to 100 °C in EDTA buffer (pH = 8.0).

For western blot analysis, 10% brain homogenates were prepared in 0.32 M sucrose using a Precellys24 (Bertin). Extracts of 50-90 μg protein were digested with 50 $\mu\text{g}/\text{ml}$ proteinase-K (PK) in DOC/NP-40 0.5% for 45 minutes at 37 °C. The reaction was stopped by adding 3 μl complete protease inhibitor cocktail and 8 μl of a lauryl dodecyl sulfate (LDS)-based sample buffer.

MTS assay – The MTS assay (PROMEGA) was performed according to the instructions given by the manufacturer.

Conformational stability assays – Two aliquots of RML6 brain homogenate were normalized to 2 mg ml^{-1} protein and PTAA was added to obtain final concentrations of 0, 10 or 100 $\mu\text{g ml}^{-1}$ before the samples were incubated for 30 min at 37°C on a thermoshaker rotating at 700 rpm. Aliquots of 10 μl containing 20 μg protein each were prepared and two times diluted with either water or different concentrations of GdnHCl. The samples were incubated for 10 min at room temperature prior to analysis by Western blot or MPA. For Western blot analysis, the samples were digested with PK (15 $\mu\text{g}/\text{ml}$) and 20 μl of the samples were separated on a 12% Bis-Tris SDS polyacrylamide gel (NuPAGE, Invitrogen) followed by blotting onto a

nitrocellulose membrane. For MPA analysis, samples without or with 10 $\mu\text{g ml}^{-1}$ PTAA were diluted 1:100 in TBSTT prior to the capture with peptoid-coated beads and MPA was performed as described above.

ELISA – Homogenates from COCS were diluted ten-fold in TBSTT to obtain a final concentration of 0.1 mg ml^{-1} total protein. Digestion with PK was performed in a 96-well plate for 60 min at 37°C, rotating at 700 rpm on a thermoshaker in a total volume of 50 μl containing 50 $\mu\text{g ml}^{-1}$ PK. Digestion was stopped by adding 2 mM phenylmethanesulfonylfluoride (PMSF, Calbiochem) and Complete Mini protease inhibitor cocktail (Roche). Digested samples were denatured with an equal volume of 3 M GdnSCN for 30 min at 37°C and diluted with four volumes of 0.1 M NaHCO_3 , pH 8.9. The samples were then detected by sandwich ELISA. Briefly, ELISA plates were coated with POM1-antibodies (400 ng/well) in coating buffer over night. After washing with PBST, plates were blocked with blocking buffer (5% TopBloc in PBST) for 2 h at room temperature. Next, samples were incubated for 2 hours on ELISA plates (Nunc, MaxiSorb). Captured samples were detected with biotinylated POM19 antibody (1 $\mu\text{g ml}^{-1}$, 1 h, diluted in sample buffer) and horseradish peroxidase (HRP)-avidin conjugate (1 $\mu\text{g ml}^{-1}$, 1 h, diluted in sample buffer) (BD Pharmingen). Samples were analysed by ELISA in technical triplicates and washed five times with PBS 0.05% Tween20 between each antibody and conjugate incubations. The development was performed either calorimetrically or by chemiluminescence. For the calorimetric detection, TMB substrate (Invitrogen) was added to the wells and incubated for 15 min at room temperature and stopped by adding 0.5 M H_2SO_4 . The absorbance was read at 450 nm by VERSAmax microplate reader and validated with SOFTmax PRO software. For chemiluminescence, the chemiluminescent substrate (Thermo Scientific) was added to the wells and incubated for 3 min at room temperature. The relative light units were measured with a luminometer (~425nm) and validated with SOFTmax PRO software.

Preparation of recombinant mouse mPrP²³⁻²³¹ and fibril formation – Recombinant mouse PrP comprising residues 23-231 was expressed and purified as described elsewhere (78-80). mPrP²³⁻²³¹ fibers were produced by incubating the protein in 50 μM Tris-HCl, 1 M GdnHCl, 150

mM sodium chloride, pH 7.5, for 48 h at 37 °C and shaking at 600 rpm (45). To study the inhibition of fiber formation by PTAA, mPrP₂₃₋₂₃₁ fibers were grown in the absence and presence of different concentrations of PTAA ranging from 1 to 50 µg ml⁻¹. The time course of fiber formation was followed by measuring the optical density at 350 nm on a Tecan Saphire 2 plate reader. After 48h the samples were also analysed by transmission electron microscopy. Preformed fibrils were mixed with PTAA at concentrations of 10, 25, 50 and 100 µg ml⁻¹ PTAA for 30 min at 37°C and shaking at 600 rpm prior to analysis by transmission electron microscopy.

Transmission electron microscopy – Carbon coated copper grids were placed on 10 µl of the fibril solutions and incubated for 1 min. After removing of excess liquid, grids were washed three times with water prior to staining with 2% aqueous uranyl acetate for 1 min. Samples were analysed on a Philips CM12 electron microscope (transmission electron microscope with an acceleration voltage of 80 keV).

Proteolysis of mPrP₂₃₋₂₃₁ fibers in the presence of PTAA – mPrP₂₃₋₂₃₁ fibers were incubated in the absence and presence of 10 µg ml⁻¹ PTAA at 37°C for 60 min on a thermoshaker rotating at 700 rpm. 18 µl of non-treated and PTAA treated fibers were digested with PK at concentrations of 0.5, 1, 1.5 and 2 µg ml⁻¹ diluted in PBS for 60 min at 37°C on a thermoshaker rotating at 700 rpm. PK digestion was terminated by adding 7 µl of 4x LDS loading buffer (NuPAGE, Invitrogen) and boiling the samples at 95 °C for 5 min. Samples were then analysed by immunoblotting.

Histagged mPrP₂₃₋₂₃₁ purification and fibril formation for the fluorescence assay – Histagged mPrP₂₃₋₂₃₁ was purified by affinity chromatography and size exclusion chromatography as described previously (81). Fibrils were generated by unfolding the protein in 6 M GdnHCl followed by partial refolding by dilution to 1 M GdnHCl and 3 M urea and 5 µM mPrP₂₃₋₂₃₁ at pH 7.3. The protein samples were shaken vigorously at 37 °C for 24 h.

Native and fibrillated mPrP₂₃₋₂₃₁ was serially two-fold diluted in several steps in a 96 well plate (Corning 3880) and PTAA was added to a final concentration of 0.2 µM. The samples were excited at 430 nm and emission spectra were recorded from 470 and 600 using a Safire II plate

reader (Tecan). Fluorescence polarization was determined by excitation at 470 nm and measuring the emission at 520 nm. The anisotropy was calculated as $r = (I_{\parallel} - I_{\perp}) / (I_{\parallel} + 2I_{\perp})$ where r is the anisotropy, I_{\parallel} is the parallel intensity and I_{\perp} is the perpendicular intensity.

Statistical analysis – For MPA presented in Figs 2, 4 and S11, technical quadruplicates were compared for each individual sample using a T-test. In Fig. 2A, the overall effect of individual LCPs was investigated by comparing a group of four concentrations of each individual polythiophenes using a post-Hoc T-test for analysis of variance.

For the SCEPA presented in Figs 2 and 4 and supplemental Fig. S7, proportion of negative wells over dilutions were compared between drugs using a Mantel-Haenszel Chi-square test with a Bonferroni-Holm correction. Confidence interval for common odds ratio is given in the respective tables for non-significant comparisons.

For Fig. 4B, P-values were calculated with a one-sample T-test comparing TCI₅₀ difference to control (homogenates from COCS of non-treated cultures harvested after 42 dpi). For Fig. 4C statistical differences were computed to compare each set of biological replica to the control homogenates from COCS with a one-way ANOVA.

RESULTS

LCPs stabilize PrP^{Sc} against proteolysis. In a first set of experiments, we screened a broad range of LCPs with various side chains and/or polymer length for their effects onto the stability of PrP^{Sc} to hydrolysis by PK. The compounds tested included polydisperse LCPs such as the anionic PTAA (24,26,29,30), the cationic POMT (26,29,30) and PTMI (31), the zwitterionic PBAT (supplemental Fig. S1) and POWT (30,32,33). We then tested monodisperse LCPs such as the anionic compounds pHTAA and pFTAA (34,35) (Fig. 1A). All LCPs are charged at physiological pH.

We mixed a 1% brain homogenate obtained from mice infected with RML6 prions (Rocky Mountain Laboratory strain, passage 6) with each LCP (1-900 µg ml⁻¹). Samples were incubated for 30 min at 37°C in an orbital shaker (700 rpm). Samples were then digested with 50 µg ml⁻¹ PK and analyzed by immunoblotting. Treatment with

each LCP (except tPOWT) was found to increase the PK resistance of PrP^{Sc} in a concentration-dependent manner and to induce the formation of SDS-stable aggregates (Fig. 1B). PBAT and POWT were less effective at enhancing the PK resistance of PrP^{Sc}, but augmented the formation of oligomeric SDS-stable PrP^{Sc} aggregates. Longer exposures of the blots revealed that these aggregates were enhanced by all LCPs (Fig. 1B and supplemental Fig. S2). We also used PPS as control. PPS did not show any effect on PK resistance up to a concentration of 10 $\mu\text{g ml}^{-1}$, whereas the LCPs had a strong effect at the same concentration (supplemental Fig. S3).

To investigate the limit of the LCP-induced enhancement of PK resistance, we performed a digestion with a 40-fold higher concentration of PK on PTAA-treated RML6 and doubled the incubation time of proteolysis. The signal for untreated PrP^{Sc} was completely abolished, yet PTAA-treated PrP^{Sc} remained detectable even under these harsh conditions (supplemental Fig. S4). Exposure of RML6 to extremely high PTAA and POMT concentrations ($>50 \mu\text{g ml}^{-1}$) reduced the levels of PrP^{Sc} (Fig. 1B and Fig. 4A). Hence, PTAA and POMT in extremely high concentrations may partially destabilize the protein aggregates.

We performed several experiments to assess whether the presence of the LCPs compromised the assay used for assessing PK resistance, thereby leading to artifactual results. To investigate whether LCPs interfere with the enzymatic activity of PK, we PK-digested non-infectious CD1 brain homogenates in the absence or presence of PTAA. We did not observe any effect of PTAA onto the efficiency of PrP^C proteolysis (supplemental Fig. S5A and B). Next, we tested whether the addition of PTAA to PK-predigested RML6 homogenate affects the level of PrP^{Sc}. The PrP^{Sc} signal increased only when proteolysis of RML6 prions was performed after exposure with PTAA, but not when PTAA was added a posteriori (supplemental Fig. S6). We conclude that LCPs indeed increase the resistance of PrP^{Sc} to PK by directly modifying the properties of PrP^{Sc}.

LCPs reduce prion infectivity in brain homogenates – We then asked whether LCPs can reduce prion infectivity titers. We mixed 1% brain homogenate obtained from mice infected with RML6 prions with LCPs ($300 \mu\text{g ml}^{-1}$) for 30 min at 37°C. Prion infectivity was then quantified by

assessing $\text{TCI}_{50} \text{ g}^{-1}$ (number of units transmitting infectivity to tissue cultures with 50% likelihood per gram of brain homogenate) with the Scrapie Cell End-Point Assay (SCEPA) (36). All LCPs significantly reduced infectivity in RML6 homogenates against non-treated RML6 homogenate ($\log \text{TCI}_{50} \text{ g}^{-1} > 7.9 \pm 0.3$; Fig. 2A and supplemental Table S1). Due to their high activity, PTAA and its monodisperse counterpart pFTAA were further investigated in a titration assay. PTAA reduced infectivity in RML6 brain homogenates by 3 logs $\text{TCI}_{50} \text{ g}^{-1}$ at $900 \mu\text{g ml}^{-1}$, and completely abated infectivity at $5000 \mu\text{g/ml}$. The effect of pFTAA on prion infectivity appeared similar to that of PTAA (Fig. 2B and C).

The validity of the SCEPA is unaffected by LCPs. Next, we asked whether residual LCPs may affect the susceptibility of N2a-PK1 cells to prions, thereby producing artifactually optimistic results. In a first experiment a 10-fold excess of RML6 homogenate was added to RML6 samples treated, or non-treated, with $500 \mu\text{g ml}^{-1}$ PTAA (supplemental Fig. S7). The resulting prion titers were similar to those of non-treated RML6 homogenates, whereas the PTAA-treated control sample exhibited decreased titers (supplemental Tables S2). Hence PTAA did not decrease the susceptibility of N2a-PK1 cells to prion infection, or the readout of the SCEPA. In a second experiment we tested whether preincubation of N2a-PK1 cells with PTAA would affect the susceptibility of cells to prion infection (supplemental Fig. S7). We supplemented the culture medium before infection with $10 \mu\text{g ml}^{-1}$ PTAA, which corresponds to the PTAA concentration in the medium used for the RML6 infection treated with $900 \mu\text{g ml}^{-1}$ (Fig. 2B). Prion titration by SCEPA yielded comparable $\text{TCI}_{50} \text{ g}^{-1}$ values (supplemental Tables S3), confirming that the susceptibility of the cells to prion infection was not affected by the treatment with PTAA. We conclude that the PTAA-treated cells remained fully susceptible to RML6. Hence the observed decrease in infectivity in PTAA-treated sample represented a true PTAA-induced reduction of prion infectivity.

Finally, cell viability was tested to exclude the possibility of acute toxicity of PTAA to N2a-PK1 cells when supplemented into the culture medium (supplemental Fig. S8). PTAA at the highest dose of $45 \mu\text{g ml}^{-1}$ used in our study did not affect cell viability. Therefore LCP can suppress prion

infectivity of brain homogenates below the SCEPA detection limit without affecting the sensitivity of the assay.

LCPs decrease the concentration of PrP aggregates – Because PK resistance is often used as a surrogate marker of prion infectivity, the finding that LCPs reduce infectivity while rendering PrP^{Sc} more resistant to PK digestion was counterintuitive. We therefore used the Misfolded Protein Assay (MPA) to further analyze the physical properties of LCP-treated prions. The MPA enables sensitive and quantitative detection of prion aggregates without the use of PK (37-39). Paramagnetic beads coated with prion-specific binding peptoids selectively capture PrP aggregates, whereas monomeric PrP is not captured. Captured PrP is then eluted and detected by enzyme-linked immunosorbent assay (ELISA) using the PrP-specific antibody POM19 (40).

To evaluate the sensitivity of the MPA, beads were incubated with 10-fold serial dilutions (10^{-3} to 10^{-10}) of a 10% (wt/vol) RML6 brain homogenate, and intracerebrally inoculated into tga20 mice overexpressing PrP^C (41) (supplemental Table S4). Mice developed clinical signs after mean incubation times of 78-106 days (supplemental Table S4). Spongiform encephalopathy was confirmed in all clinically diseased mice by histopathological and immunohistochemical analysis (supplemental Fig. S9). Besides confirming a linear relationship between infectivity and MPA readings, these results show that peptoid-coated beads capture prion infectivity efficiently from RML6 and transmit it to tga20 mice. These data suggest that the MPA readings reflect the number of prion seeds present in a sample.

We then mixed 1% RML6 brain homogenate with PTAA, POMT, pHTAA or pFTAA. These LCPs were chosen because they showed the strongest effect on infectivity in the SCEPA. All four compounds affected the aggregational state of PrP^{Sc} dose-dependently (Fig. 2D). Treatment of RML6 with $10 \mu\text{g ml}^{-1}$ PTAA, POMT and pFTAA significantly reduced the MPA signal ($p = 0.004$, 0.015 and 0.003 , respectively, supplemental Table S5). PTAA and POMT had the strongest effect at 300 and $100 \mu\text{g ml}^{-1}$, respectively, whereas pFTAA was more efficient at 1 and $10 \mu\text{g ml}^{-1}$. Already the treatment with $1 \mu\text{g ml}^{-1}$ pFTAA caused a significant reduction in

the MPA signal ($p = 0.028$; supplemental Table S5). We then pre-incubated beads with $100 \mu\text{g ml}^{-1}$ PTAA. Pretreatment of the beads had no effect on the capture efficiency of non-treated or PTAA-treated RML6 prions (supplemental Fig. S10 and supplemental Table S6), indicating that LCPs do not affect the assay by interacting nonspecifically with peptoid-coated paramagnetic beads.

PTAA alters the conformational stability of PrP^{Sc} – We next investigated whether PTAA changes the biochemical properties of RML6 prions by altering the conformational stability of PrP^{Sc}. Non-treated and PTAA-treated RML6 brain homogenates were incubated with increasing concentrations of GdnHCl for 60 min, digested with PK to remove soluble PrP, and analyzed by immunoblotting for PrP^{Sc} (42). PTAA treatment strongly increased the sensitivity of PrP^{Sc} to denaturation with GdnHCl, as reflected by a shift in the concentration of GdnHCl required for loss of PK resistance (3 M for non-treated sample, and 2.4 and 2 M for samples exposed to 10 and $100 \mu\text{g ml}^{-1}$ PTAA, respectively; Fig. 3A).

We also incubated native and PTAA-treated RML6 with various concentrations of GdnHCl and quantified the amount of aggregated PrP by MPA (Fig. 3B). The inflexion point of the transition curve, where 50% of aggregated PrP is captured by the peptoids, was 1.72 M GdnHCl for non-treated RML6 and 0.31 M GdnHCl for PTAA-treated RML6. Hence PTAA-treated RML6 brain homogenate was more sensitive to GdnHCl denaturation than non-treated homogenate, indicating that PTAA physically changes the stability of PrP^{Sc} against chaotropic salts.

PTAA antagonizes prion infection in cerebellar organotypic cultured slices – We then evaluated the antiprion activity of LCPs ex vivo in a complex cellular environment. For that, we used the prion organotypic slice culture assay (POSCA) (43,44). We used again PTAA as lead compound to determine the impact of LCPs onto prion replication and accumulation in the POSCA. Cerebellar organotypic cultured slices (COCS) were prepared from 11 days-old PrP^C-overexpressing tga20 pups and kept in culture for 42 days (43). Cultures were analyzed for the presence of PrP^{Sc} at 21 days post inoculation (dpi) by assessing PK-resistant material on immunoblots (Fig. 4A). PTAA was added to the culture medium at 21 dpi at each medium

exchange (10 ng to 60 $\mu\text{g ml}^{-1}$). Slices were harvested at 42 dpi, and the impact of PTAA was analyzed with the tools described above.

We first compared the amounts of PrP^{Sc} between non-treated and PTAA-treated slices by PK digestion and immunoblotting (Fig. 4A). As in PTAA-treated RML6 brain homogenates, we observed a substantial, dose-dependent increase in PrP^{Sc} (Fig. 4A) and high-molecular weight PrP aggregates. Treatment with the highest PTAA concentration (60 $\mu\text{g ml}^{-1}$) again lowered the amount of PrP^{Sc} below detectability. PPS, which effectively inhibited PrP^{Sc} replication in prion-infected COCS (43), was used as control. In contrast to slices exposed to PTAA, PPS (0.3 $\mu\text{g ml}^{-1}$) strongly reduced PrP^{Sc} when compared to non-treated controls. Untreated or PTAA-treated slices exposed to non-infected brain homogenates from CD1 mice, did not contain any PrP^{Sc} .

We next investigated the effect of PTAA on prion replication in COCS (43). During the interval between 21 and 42 dpi prions were amplified in RML6-infected slices, as evidenced by an increase in infectivity from 5.7 to 7.4 $\log \text{TCI}_{50} \text{ g}^{-1}$ (1 TCI_{50} unit being the dose required to infect 50% of PK1 culture wells; Fig. 4B). When slices were exposed to PTAA, a dose-dependent reduction in infectivity was observed. Infectivity was reduced by $>3 \log \text{TCI}_{50} \text{ g}^{-1}$ with the highest PTAA concentration of 60 $\mu\text{g ml}^{-1}$, which is $>1.5 \log \text{TCI}_{50} \text{ g}^{-1}$ below the initial infectivity at day 21 dpi ($p = 0.012$, $p = 0.001$ and $p < 0.001$; respectively, supplemental Table S7). Treatment with PPS at a concentration of 0.3 $\mu\text{g ml}^{-1}$ was as efficient as treatment with 6 $\mu\text{g ml}^{-1}$ PTAA and resulted in a reduced infectivity of $>2 \log \text{TCI}_{50} \text{ g}^{-1}$ when compared to non-treated cultures at 42 dpi. A comparison of MPA readings (Fig. 4C) and SCEPA results (Fig. 4B) shows that the quantification of PrP aggregates in the various samples exactly reflected the data obtained from the SCEPA, again confirming a close relationship between the number of PrP aggregates and prion infectivity (Fig. 4F).

To further validate the potency of PTAA on RML6-infected slice cultures, we developed a sandwich ELISA using antibodies POM1 for coating and POM19 for detection. This allowed us to simultaneously quantify the levels of total PrP ($\text{PrP}^{\text{C}} + \text{PrP}^{\text{Sc}}$) and PrP^{Sc} in slice homogenates (Fig. 4D). Homogenates from non-treated slices harvested at days 21 and 42 dpi contained

1.2 ± 1.0 and $42.9 \pm 14.6 \text{ ng PrP}^{\text{Sc}}$ per gram total protein. The levels of PrP^{Sc} in PTAA treated slices significantly declined with increasing concentrations of PTAA, and strongly correlated with the SCEPA and MPA data (Fig. 4G and H). A comparison of the ELISA data with the immunoblot indicated that the high molecular-weight aggregates may not be detected in the ELISA, probably due to their resistance to denaturation with GdnSCN which prevents the exposure of buried epitopes.

Treatment with PTAA (60 $\mu\text{g ml}^{-1}$) suppressed PrP^{Sc} to values below detectability by ELISA (supplemental Table S8). Homogenates from cultures treated with 0.3 $\mu\text{g ml}^{-1}$ PPS showed levels of PrP^{Sc} similar to the homogenates at day 21 dpi and to COCS treated with PTAA at 6 $\mu\text{g ml}^{-1}$. No PrP^{Sc} was detectable in uninfected controls. To test whether PTAA acts directly on PrP^{C} , we quantified the PrP^{C} levels in the various samples by subtracting the amount of PrP^{Sc} from total PrP (Fig. 4E). The amount of PrP^{C} was unaffected in all samples except for slices treated with 60 $\mu\text{g ml}^{-1}$ PTAA which showed a significant reduction in PrP^{C} levels.

PTAA treatment efficiently inhibits prion replication – To evaluate the efficiency of PTAA as a post-exposure regimen in slice cultures, we first generated a time-dependent standard curve for prion accumulation. Prion-infected slice cultures were harvested at days 0, 7, 19, 21, 28, 35 and 42 dpi, and prion aggregates were analyzed by MPA and by sandwich ELISA after PK digestion. Prion aggregates and PrP^{Sc} were hardly detectable until 21 dpi (Fig. 5A and B), and newly formed PrP^{Sc} accumulated gradually thereafter and reached a plateau after 45 days. Prion accumulation was completely suppressed by 10 $\mu\text{g ml}^{-1}$ PTAA if treatment was initiated before day 21 dpi. If treatment was started at 28 dpi, a conspicuous inhibitory effect of PTAA was observed with reduction of PrP aggregates below the detection limit of the MPA and a strong decline in PrP^{Sc} when compared to non-treated prion-infected homogenates.

A direct comparison of MPA and ELISA shows that the quantification of PrP aggregates with the prion-specific binding peptoids was less sensitive than the sandwich ELISA in this paradigm. Perhaps the proximal coating of PrP aggregates with PTAA interfered with the interaction between peptoids and binding sites on

PrP aggregates. Alternatively, PTAA might induce a structural rearrangement of the aggregates into larger associations that reduces the surface available for binding to the peptoid-coated beads.

We also evaluated the levels of PrP^C in homogenates (Fig. 5C). PrP^C levels were reduced about two fold compared to non-treated samples independent from the time point at which treatment was started. This confirms further that PTAA treatment might affect prion accumulation by reducing the amount of PrP^C, or of a transition intermediate on-path towards PrP^{Sc}.

PTAA inhibits fibrillogenesis of recombinant PrP and affects pre-formed recombinant PrP fibers – We used an in vitro conversion assay to address the mode of action of the LCPs on prion replication and accumulation in a well-defined, simple environment. We first investigated whether PTAA inhibits amyloid fiber formation of the recombinant mouse prion protein mPrP₂₃₋₂₃₁. Monomeric mPrP₂₃₋₂₃₁ was grown under slightly denaturing conditions (45) in the presence of PTAA, and the time course of fiber formation was assessed by optical density measurements at 350 nm for 48h. mPrP₂₃₋₂₃₁ formed amyloid-like fibers by nucleation-dependent polymerization with a lag phase followed by an exponential growth phase and a plateau (Fig. 6A). The addition of PTAA significantly reduced the growth rate of fibers in a concentration-dependent manner (Fig. 6A); incubation with 50 $\mu\text{g ml}^{-1}$ resulted in a complete inhibition of fiber formation.

We further analyzed the samples by negatively-stained transmission electron microscopy (TEM) (Fig. 6B). Electron micrographs (EM) of non-treated control samples taken after 48h showed long unbranched fibers, whereas fibers grown in the presence of PTAA (1-10 $\mu\text{g ml}^{-1}$) appeared coated with globular, regularly spaced PTAA aggregates. Quantitative analysis revealed that PTAA forms two different populations of aggregates with average diameters of 43.9 ± 6.1 nm and 16.8 ± 2.5 nm when bound to the fibers compared to 25.6 ± 7.4 nm and 15.4 ± 2.7 nm for the free aggregates. Both populations bind to the fibers with a recognizable periodicity (Fig. 6D, E and F), suggesting that PTAA interacts specifically with defined binding sites on the fibers. In addition, we partially observed coalescence of the fibers into more compact structures at these concentrations. Empty EM

grids at high doses of PTAA confirmed the strong inhibitory effect of PTAA (Fig. 6B).

The presence of compact fiber conglomerates in the samples grown in the presence of PTAA at concentrations between 1 and 10 $\mu\text{g ml}^{-1}$ prompted us to ask whether PTAA also interacts directly with existing mPrP₂₃₋₂₃₁ fibers. We therefore incubated preformed fibers with PTAA and analyzed their morphology by TEM. Similarly to the fibers grown in the presence of PTAA, fibers incubated with PTAA at concentrations between 1 and 10 $\mu\text{g ml}^{-1}$ were associated with small aggregates of PTAA (Fig. 6C and D). With increasing PTAA concentrations we observed progressive coating and agglomeration of fibers (Fig. 6C).

We then asked whether PTAA directly interacts with native mPrP₂₃₋₂₃₁. Native mPrP₂₃₋₂₃₁ was serially diluted and 0.2 μM PTAA was added to all samples. Fluorescence intensity and fluorescence polarization were measured (supplemental Fig. S11). PTAA was quenched by native mPrP₂₃₋₂₃₁, suggesting that the probe binds also native PrP^C or a transition intermediate on-path towards aggregating.

To validate that the increased PK-resistance of PrP^{Sc} in PTAA treated RML6 brain homogenates and prion-infected slice cultures can be ascribed to a direct interaction of PTAA on PrP^{Sc} independently of the sample environment, we investigated whether PTAA also renders mPrP₂₃₋₂₃₁ fibers more stable to PK digestion. mPrP₂₃₋₂₃₁ fibers were incubated with 10 $\mu\text{g ml}^{-1}$ PTAA prior to limited proteolysis with different PK concentrations and immunoblotting. Fig. 6G displays that PTAA directly acts on PrP as evidenced by a significant increase in PK resistance of recombinant mPrP₂₃₋₂₃₁ fibers. We conclude that PTAA prevents prion replication and accumulation by acting on both PrP^C and PrP^{Sc} aggregates in a concentration-dependent manner.

DISCUSSION

We had previously found that LCPs interact with amyloids, including PrP^{Sc}. The fluorescent spectra emanating from PrP^{Sc}-complexed LCPs allowed for differentiation of prion strains, suggesting a remarkable degree of steric specificity (28). These observations prompted us

to explore whether additional biophysical properties of prions, such as the stability of PrP^{Sc} aggregates and their infectiousness, may be affected by interactions with LCPs. The ultimate hope would be that these experiments might identify the polythiophene scaffold as a novel pharmacophore for the treatment of protein aggregation diseases.

Indeed, not only did LCP treatment of infectious brain homogenates significantly reduce their infectivity, but also prion-infected organotypic slice cultures accrued less infectivity when exposed to LCPs. Several polythiophenes with diverse charged side chains and backbone lengths were able to reduce infectivity when added to prion-containing brain homogenates. The antiprion activity of these compounds cannot be attributed to the charges of their side chains, since anionic, cationic and zwitterionic compounds reduced prion infectivity to a similar extent. Also, neither the spacing between the side chains nor the rigidity of the molecules seemed to play a role for their antiprion activity. Based on theoretical considerations, the total avidity of LCPs for amyloids should increase with the number of low-affinity binding sites, and therefore with the length of the polymers. However, very long polymers may have chemical properties limiting their interactions. Hence the activity of LCPs appears to be an intrinsic property of the polythiophene backbone itself.

The mode of action of LCPs may involve more than one mechanism. When used at low concentrations the LCPs appear to render PrP^{Sc} more stable to PK digestion and to induce the formation of SDS-stable high-molecular-weight aggregates. Accordingly, PTAA transformed recombinant mPrP₂₃₋₂₃₁ fibers into more compact structures. At extremely high concentrations, PTAA and POMT, however, significantly decreased the resistance of PrP^{Sc} to PK. PTAA also caused a left-shift in the conformational stability curve of PrP^{Sc} after exposure to increasing concentrations of the non-surfactant-type chaotrope, GdnHCl. This concentration-dependent behavior of the LCPs resembles the mechanisms reported for several surfactants which were assumed to affect protein aggregation in a two-concentration regime by either interacting as single molecules or in equilibrium with small molecule aggregates (46) and were demonstrated to enhance or reduce the stability and detectability of PK resistant PrP^{Sc} (18,47,48).

The concentration-dependent interaction of surfactants with aggregated proteins may induce conformational versatility. Low concentrations of SDS and LiDs were shown to act like negatively charged lipid interfaces favoring the formation of global hydrogen bonding, thereby facilitating the formation of β -sheet structure and e.g. promoting A β self-assembly (49-52), whereas micellar SDS inhibits aggregation by enhancing α -helical conformational states (53). A similar mode of action was reported for CR which induces β -sheet formation and self-propagation of monomeric A β (54,55). LCPs might therefore act similarly to membrane mimetics that promote de novo PrP aggregation by converting PrP into compact aggregates that are more resistant to PK but less infectious.

Accordingly, LCPs used at submicellar concentrations may prevent prion replication by hyperstabilization of the PrP^{Sc} conformation, resulting in reduced fiber frangibility – a critical determinant of prion infectivity (56,57) which controls prion propagation by fragmentation of fibrils and elongation of these infectious seeds into new fibrils (58). The higher compactness of LCP-treated PrP^{Sc} aggregates may reduce the release of infectious particles, resulting in decreased prion infectivity. This scenario is supported by studies suggesting that large aggregates do not correlate well with high infectivity (59-61). Hence LCPs can be protective by stabilizing fragile fibrils and perhaps even by incorporating pre-existing prions, and possibly also PrP^C, into inert structures (Fig. 7).

The PK resistance of PrP^{Sc} is widely accepted as surrogate marker for prion infectivity and is often used for the screening of novel compounds for the treatment of prion diseases. However, we found a glaring dissociation between these two parameters. Along with previous observations (48,62-68), these findings question the use of PK resistance as the sole screening parameter. Alternative methods, such as the MPA, appear to better reflect prion infectivity and may be better suited to screening for novel antiprion compounds.

While the above data indicates that LCPs can interact with PrP^{Sc}, their antiprion effects on COCS suggest that LCPs may intervene at additional steps during the transition process of PrP^C to PrP^{Sc}. In particular, ELISA measurements on COCS showed reduced levels of PrP^C, suggesting that PTAA might deplete PrP^C from

the cell surface or modulate PrP^C levels in prion trafficking. This may reduce the amount of PrP^C accessible for the transition of PrP^C into PrP^{Sc}. A similar mode of action was reported for other antiprion compounds (48,69-75). This interpretation is supported by our finding of a direct interaction of PTAA with PrP^C by performing an in vitro conversion assay with recombinant mPrP₂₃₋₂₃₁ in the presence of PTAA in a cell-free environment. PTAA strongly inhibits the formation of mPrP₂₃₋₂₃₁ fibers, supporting that PTAA directly interact with PrP^C by either stabilizing the spatial conformation of PrP^C or protecting the binding site for the template PrP^{Sc} molecule. Both effects may prevent efficient transition of PrP^C into PrP^{Sc}.

In conclusion, the interaction of the LCPs with PrP^{Sc} causes a structural transformation in a surfactant like manner mostly independent of the molecular character of the LCPs. The treatment renders PrP^{Sc} more resistant to PK digestion without affecting proteolysis of PrP^C, and profoundly reduces prion infectivity. The data presented above link these effects to the hyperstabilization of PrP^{Sc}. Therefore, LCPs may represent a promising new class of antiprion compounds. The newly developed LCPs, pHTAA and pFTAA, were shown to cross the BBB (34) and may represent promising candidates for further exploration and for in vivo studies.

REFERENCES

1. Mastrianni, J. A. (2010) *Genet Med* 12, 187-195
2. Edgeworth, J. A., Gros, N., Alden, J., Joiner, S., Wadsworth, J. D., Linehan, J., Brandner, S., Jackson, G. S., Weissmann, C., and Collinge, J. (2010) *Proc Natl Acad Sci U S A* 107, 14402-14406
3. Weissmann, C., Enari, M., Kohn, P. C., Rossi, D., and Flechsig, E. (2002) *J Infect Dis* 186 Suppl 2, S157-165
4. Aguzzi, A., and Polymenidou, M. (2004) *Cell* 116, 313-327
5. Haybaeck, J., Heikenwalder, M., Klevenz, B., Schwarz, P., Margalith, I., Bridel, C., Mertz, K., Zirdum, E., Petsch, B., Fuchs, T. J., Stitz, L., and Aguzzi, A. (2011) *PLoS Pathog* 7, e1001257
6. Prusiner, S. B. (1998) *Proc Natl Acad Sci U S A* 95, 13363-13383
7. Weissmann, C. (2004) *Nat Rev Microbiol* 2, 861-871
8. Aguzzi, A., and Calella, A. M. (2009) *Physiol Rev* 89, 1105-1152
9. Aguzzi, A. (2009) *Nature* 459, 924-925
10. Appleby, B. S., and Lyketsos, C. G. (2011) *Expert Opin Pharmacother* 12, 1-12
11. Korth, C., May, B. C., Cohen, F. E., and Prusiner, S. B. (2001) *Proc Natl Acad Sci U S A* 98, 9836-9841
12. Pocchiari, M., Schmittinger, S., and Masullo, C. (1987) *J Gen Virol* 68 (Pt 1), 219-223
13. Collinge, J., Gorham, M., Hudson, F., Kennedy, A., Keogh, G., Pal, S., Rossor, M., Rudge, P., Siddique, D., Spyer, M., Thomas, D., Walker, S., Webb, T., Wroe, S., and Darbyshire, J. (2009) *Lancet Neurol* 8, 334-344
14. Martinez-Lage, J. F., Rabano, A., Bermejo, J., Martinez Perez, M., Guerrero, M. C., Contreras, M. A., and Lunar, A. (2005) *Surg Neurol* 64, 542-545, discussion 545
15. Benito-Leon, J. (2004) *Clin Neuropharmacol* 27, 201-203
16. Ingrosso, L., Ladogana, A., and Pocchiari, M. (1995) *J Virol* 69, 506-508
17. Tagliavini, F., McArthur, R. A., Canciani, B., Giaccone, G., Porro, M., Bugiani, M., Lievens, P. M., Bugiani, O., Peri, E., Dall'Ara, P., Rocchi, M., Poli, G., Forloni, G., Bandiera, T., Varasi, M., Suarato, A., Cassutti, P., Cervini, M. A., Larsen, J., Salmona, M., and Post, C. (1997) *Science* 276, 1119-1122
18. Caspi, S., Halimi, M., Yanai, A., Sasson, S. B., Taraboulos, A., and Gabizon, R. (1998) *J Biol Chem* 273, 3484-3489
19. Ouidja, M. O., Petit, E., Kerros, M. E., Ikeda, Y., Morin, C., Carpentier, G., Barritault, D., Brugere-Picoux, J., Deslys, J. P., Adjou, K., and Papy-Garcia, D. (2007) *Biochem Biophys Res Commun* 363, 95-100
20. Tsuboi, Y., Doh-Ura, K., and Yamada, T. (2009) *Neuropathology* 29, 632-636
21. Terada, T., Tsuboi, Y., Obi, T., Doh-ura, K., Murayama, S., Kitamoto, T., Yamada, T., and Mizoguchi, K. (2010) *Acta Neurol Scand* 121, 127-130
22. MacGregor, I. R., Dawes, J., Pepper, D. S., Prowse, C. V., and Stocks, J. (1985) *Thromb Haemost* 53, 411-414
23. Supattapone, S., Piro, J. R., and Rees, J. R. (2009) *CNS Neurol Disord Drug Targets* 8, 323-328
24. Nilsson, K. P., Herland, A., Hammarstrom, P., and Inganas, O. (2005) *Biochemistry* 44, 3718-3724
25. Herland, A., Nilsson, K. P., Olsson, J. D., Hammarstrom, P., Konradsson, P., and Inganas, O. (2005) *J Am Chem Soc* 127, 2317-2323
26. Nilsson, K. P., Hammarstrom, P., Ahlgren, F., Herland, A., Schnell, E. A., Lindgren, M., Westermark, G. T., and Inganas, O. (2006) *ChemBiochem* 7, 1096-1104

27. Nilsson, K. P., Ikenberg, K., Aslund, A., Fransson, S., Konradsson, P., Rocken, C., Moch, H., and Aguzzi, A. (2010) *Am J Pathol* 176, 563-574
28. Sigurdson, C. J., Nilsson, K. P., Hornemann, S., Manco, G., Polymenidou, M., Schwarz, P., Leclerc, M., Hammarstrom, P., Wüthrich, K., and Aguzzi, A. (2007) *Nat Methods* 4, 1023-1030
29. Nilsson, K. P., Aslund, A., Berg, I., Nystrom, S., Konradsson, P., Herland, A., Inganas, O., Stabo-Eeg, F., Lindgren, M., Westermarck, G. T., Lannfelt, L., Nilsson, L. N., and Hammarstrom, P. (2007) *ACS Chem Biol* 2, 553-560
30. Aslund, A., Herland, A., Hammarstrom, P., Nilsson, K. P., Jonsson, B. H., Inganas, O., and Konradsson, P. (2007) *Bioconjug Chem* 18, 1860-1868
31. Ho, H. A., Boissinot, M., Bergeron, M. G., Corbeil, G., Dore, K., Boudreau, D., and Leclerc, M. (2002) *Angew Chem Int Ed Engl* 41, 1548-1551
32. Nilsson, K. P., Rydberg, J., Baltzer, L., and Inganas, O. (2003) *Proc Natl Acad Sci U S A* 100, 10170-10174
33. Nilsson, K. P., and Inganas, O. (2003) *Nat Mater* 2, 419-424
34. Aslund, A., Sigurdson, C. J., Klingstedt, T., Grathwohl, S., Bolmont, T., Dickstein, D. L., Glimsdal, E., Prokop, S., Lindgren, M., Konradsson, P., Holtzman, D. M., Hof, P. R., Heppner, F. L., Gandy, S., Jucker, M., Aguzzi, A., Hammarstrom, P., and Nilsson, K. P. (2009) *ACS Chem Biol* 4, 673-684
35. Aslund, A., Nilsson, K. P., and Konradsson, P. (2009) *J Chem Biol* 2, 161-175
36. Kohn, P. C., Stoltze, L., Flechsig, E., Enari, M., and Weissmann, C. (2003) *Proc Natl Acad Sci U S A* 100, 11666-11671
37. Lau, A. L., Yam, A. Y., Michelitsch, M. M., Wang, X., Gao, C., Goodson, R. J., Shimizu, R., Timoteo, G., Hall, J., Medina-Selby, A., Coit, D., McCoin, C., Phelps, B., Wu, P., Hu, C., Chien, D., and Peretz, D. (2007) *Proc Natl Acad Sci U S A* 104, 11551-11556
38. Polymenidou, M., Prokop, S., Jung, H. H., Hewer, E., Peretz, D., Moos, R., Tolnay, M., and Aguzzi, A. (2011) *Brain Pathol* 21, 209-214
39. Kranich, J., Krautler, N. J., Falsig, J., Ballmer, B., Li, S., Hutter, G., Schwarz, P., Moos, R., Julius, C., Miele, G., and Aguzzi, A. (2010) *J Exp Med* 207, 2271-2281
40. Polymenidou, M., Moos, R., Scott, M., Sigurdson, C., Shi, Y. Z., Yajima, B., Hafner-Bratkovic, I., Jerala, R., Hornemann, S., Wuthrich, K., Bellon, A., Vey, M., Garen, G., James, M. N., Kav, N., and Aguzzi, A. (2008) *PLoS One* 3, e3872
41. Fischer, M., Rulicke, T., Raeber, A., Sailer, A., Moser, M., Oesch, B., Brandner, S., Aguzzi, A., and Weissmann, C. (1996) *EMBO J* 15, 1255-1264
42. Peretz, D., Scott, M. R., Groth, D., Williamson, R. A., Burton, D. R., Cohen, F. E., and Prusiner, S. B. (2001) *Protein Sci* 10, 854-863
43. Falsig, J., and Aguzzi, A. (2008) *Nat Protoc* 3, 555-562
44. Falsig, J., Julius, C., Margalith, I., Schwarz, P., Heppner, F. L., and Aguzzi, A. (2008) *Nat Neurosci* 11, 109-117
45. Apetri, A. C., Vanik, D. L., and Surewicz, W. K. (2005) *Biochemistry* 44, 15880-15888
46. Otzen, D. E. (2010) *Curr Protein Pept Sci* 11, 355-371
47. Breyer, J., Wemheuer, W. M., Wrede, A., Graham, C., Benestad, S. L., Brenig, B., Richt, J. A., and Schulz-Schaeffer, W. J. (2012) *Vet Microbiol*, in press.
48. Milhavet, O., Mange, A., Casanova, D., and Lehmann, S. (2000) *J Neurochem* 74, 222-230
49. Rangachari, V., Reed, D. K., Moore, B. D., and Rosenberry, T. L. (2006) *Biochemistry* 45, 8639-8648
50. Tew, D. J., Bottomley, S. P., Smith, D. P., Ciccotosto, G. D., Babon, J., Hinds, M. G., Masters, C. L., Cappai, R., and Barnham, K. J. (2008) *Biophys J* 94, 2752-2766
51. Terzi, E., Holzemann, G., and Seelig, J. (1995) *J Mol Biol* 252, 633-642
52. Bokvist, M., Lindstrom, F., Watts, A., and Grobner, G. (2004) *J Mol Biol* 335, 1039-1049

53. Wahlstrom, A., Hugonin, L., Peralvarez-Marin, A., Jarvet, J., and Graslund, A. (2008) *FEBS J* 275, 5117-5128
54. Lendel, C., Bolognesi, B., Wahlstrom, A., Dobson, C. M., and Graslund, A. (2010) *Biochemistry* 49, 1358-1360
55. Abelein, A., Bolognesi, B., Dobson, C. M., Graslund, A., and Lendel, C. (2012) *Biochemistry* 51, 126-137
56. Knowles, T. P., Waudby, C. A., Devlin, G. L., Cohen, S. I., Aguzzi, A., Vendruscolo, M., Terentjev, E. M., Welland, M. E., and Dobson, C. M. (2009) *Science* 326, 1533-1537
57. Caughey, B., and Lansbury, P. T. (2003) *Annu Rev Neurosci* 26, 267-298
58. Wang, Y. Q., Buell, A. K., Wang, X. Y., Welland, M. E., Dobson, C. M., Knowles, T. P., and Perrett, S. (2011) *J Biol Chem* 286, 12101-12107
59. Gabizon, R., McKinley, M. P., and Prusiner, S. B. (1987) *Proc Natl Acad Sci U S A* 84, 4017-4021
60. Silveira, J. R., Raymond, G. J., Hughson, A. G., Race, R. E., Sim, V. L., Hayes, S. F., and Caughey, B. (2005) *Nature* 437, 257-261
61. Tixador, P., Herzog, L., Reine, F., Jaumain, E., Chapuis, J., Le Dur, A., Laude, H., and Beringue, V. (2010) *PLoS Pathog* 6, e1000859
62. Shaked, G. M., Fridlander, G., Meiner, Z., Taraboulos, A., and Gabizon, R. (1999) *J Biol Chem* 274, 17981-17986
63. Lasmezas, C. I., Deslys, J. P., Robain, O., Jaegly, A., Beringue, V., Peyrin, J. M., Fournier, J. G., Hauw, J. J., Rossier, J., and Dormont, D. (1997) *Science* 275, 402-405
64. Sklaviadis, T. K., Manuelidis, L., and Manuelidis, E. E. (1989) *J Virol* 63, 1212-1222
65. Hsiao, K. K., Groth, D., Scott, M., Yang, S. L., Serban, H., Rapp, D., Foster, D., Torchia, M., Dearmond, S. J., and Prusiner, S. B. (1994) *Proc Natl Acad Sci U S A* 91, 9126-9130
66. Piccardo, P., Manson, J. C., King, D., Ghetti, B., and Barron, R. M. (2007) *Proc Natl Acad Sci U S A* 104, 4712-4717
67. Barron, R. M., Campbell, S. L., King, D., Bellon, A., Chapman, K. E., Williamson, R. A., and Manson, J. C. (2007) *J Biol Chem* 282, 35878-35886
68. Chiesa, R., Piccardo, P., Quaglio, E., Drisaldi, B., Si-Hoe, S. L., Takao, M., Ghetti, B., and Harris, D. A. (2003) *J Virol* 77, 7611-7622
69. Shyng, S. L., Lehmann, S., Moulder, K. L., and Harris, D. A. (1995) *J Biol Chem* 270, 30221-30229
70. Enari, M., Flechsig, E., and Weissmann, C. (2001) *Proc Natl Acad Sci U S A* 98, 9295-9299
71. Perrier, V., Solassol, J., Crozet, C., Frobert, Y., Mourton-Gilles, C., Grassi, J., and Lehmann, S. (2004) *J Neurochem* 89, 454-463
72. Peretz, D., Williamson, R. A., Kaneko, K., Vergara, J., Leclerc, E., Schmitt-Ulms, G., Mehlhorn, I. R., Legname, G., Wormald, M. R., Rudd, P. M., Dwek, R. A., Burton, D. R., and Prusiner, S. B. (2001) *Nature* 412, 739-743
73. Hijazi, N., Shaked, Y., Rosenmann, H., Ben-Hur, T., and Gabizon, R. (2003) *Brain Res* 993, 192-200
74. Pauly, P. C., and Harris, D. A. (1998) *J Biol Chem* 273, 33107-33110
75. Brown, L. R., and Harris, D. A. (2003) *J Neurochem* 87, 353-363
76. Gottlieb, H. E., Kotlyar, V., and Nudelman, A. (1997) *J Org Chem* 62, 7512-7515
77. Ding, L., Jonforsen, M., Roman, L. S., Andersson, M., and Inganäs, O. (2000) *Synth Met* 110, 133-140
78. Zahn, R., Liu, A., Luhrs, T., Riek, R., von Schroetter, C., Lopez Garcia, F., Billeter, M., Calzolari, L., Wider, G., and Wüthrich, K. (2000) *Proc Natl Acad Sci U S A* 97, 145-150
79. Lysek, D. A., and Wüthrich, K. (2004) *Biochemistry* 43, 10393-10399

80. Hornemann, S., Christen, B., von Schroetter, C., Perez, D. R., and Wüthrich, K. (2009) FEBS J 276, 2359-2367
81. Almstedt, K., Nystrom, S., Nilsson, K. P., and Hammarstrom, P. (2009) Prion 3, 224-235

Acknowledgements – The authors thank Dr. B. Seifert from the Institute of Biostatistics, University of Zurich, for performing the statistical analysis, Dr. Jens Sobek from the Functional Genomics Center Zurich for his support with the Tecan Saphire 2 plate reader, Rita Moos and Ahmet Varol for technical assistance.

FOOTNOTES

*This work was supported by grants from the European Union (FP-7 Health project acronym LUPAS), the Swiss National Foundation, and the Novartis Research Foundation. AA is a recipient of an Advanced Grant of the European Research Council. KPRN is financed by an ERC Starting Independent Researcher Grant (Project: MUMID) from the European Research Council and a grant from the Swedish Foundation for Strategic Research (FFL-4).

¹To whom correspondence may be addressed: University Hospital of Zürich, Institute of Neuropathology, Schmelzbergstrasse 12, CH-8091 Zurich, Switzerland, Tel.: +41 44 255 21 07, Fax: +41 44 255 44 02, Email: Adriano.Aguzzi@usz.ch and Simone.Hornemann@usz.ch

²Department of Chemistry, University of Linköping, Sweden

³Novartis Diagnostics, 4560 Horton Street, Emeryville, CA 94608, USA

⁴The abbreviations used are: PrP, prion protein; PrP^C, cellular isoform of PrP; PrP^{Sc}, scrapie isoform of PrP^C; mPrP, mouse PrP; TSE, transmissible spongiform encephalopathy; LCP, luminescent conjugated polymer; POSCA, prion organotypic slice culture assay; COCS, cerebellar organotypic cultured slices; BBB, blood-brain barrier; RML6, Rocky Mountain Laboratory strain, passage 6; SCEPA, Scrapie Cell End-Point Assay; MPA, Misfolded Protein Assay; POSCA, prion organotypic slice culture assay; ELISA, Enzyme-linked immunosorbent assay; PTAA, Poly(thiophene-3-acetic acid); pFTAA, pentamer formyl thiophene acetic acid (4',3'''-Bis-carboxymethyl-[2,2';5',2";5",2''";5''",2''''"]quinquethiophene-5,5'''-dicarboxylic acid); pHTAA, pentamer hydrogen thiophene acetic acid (3'''-(Carboxymethyl-[2,2';5',2";5",2''";5''",2''''"]quinquethiophen-4'-yl)-acetic acid); POMT, (poly(3-[5-amino-5-methoxycarboxyl-3-oxapentyl]-2,5-thiophenylene hydrochloride); POWT, (poly(3-((S)-5-amino-5-carboxyl-3-oxapentyl)-2,5-thiophenylene) hydrochloride); PBAT, (poly-((R)-1-carboxy-N,N,N-trimethyl-2-(2-(thiophen-3-yl)ethoxy)ethanaminium)); PTMI, polythiophene methyl imidazole (poly(2-(4-methyl-3-thienyloxy)-N-ethane)N-methylimidazole chloride)

FIGURE LEGENDS

FIGURE 1. LCPs increase the resistance of PrP^{Sc} to PK digestion in RML6 brain homogenates and induce the formation of higher order aggregates. *A*, Molecular structures of LCPs. pHTAA and pFTAA are homodisperse preparations of chemically defined molecules with molecular weights of 897 and 704.7 Da, respectively. All other compounds are polydisperse preparations with average molecular weights ranging from 3000 to 11000 Da and number of monomers of n=11-20. *B*, Immunoblots of PK-digested RML6 samples after exposure with increasing doses of the different LCPs. On lane 1 in the blots of the

pHTAA and pFTAA titrations, 2 µg total protein of undigested RML6 brain homogenate was loaded as a control. On all other lanes 20 µg total protein of PK-digested non-infected (mock) or RML6-infected brain homogenate was loaded. The experiment was repeated four times with PTAA, and twice with the other LCPs. The immunoblot shown here is representative for the individual experiments. The anti-PrP antibody POM1 was used for detection. Molecular sizes are indicated in kDa.

FIGURE 2. LCPs reduce prion infectivity and the amount of prion aggregates in RML6 brain homogenates. *A*, SCEPA of RML6 homogenates mixed with the different LCPs at a concentration of 300 µg/ml. *B and C*, SCEPA of RML6 homogenates mixed with increasing concentrations of (B) PTAA and (C) pFTAA. Non-infected (mock) and RML6-infected brain homogenates were incubated with either PTAA or pFTAA and infectivity was determined on 17'000 cells in the SCEPA. Each data point represents the infectivity of one sample determined by serial tenfold dilution steps from 10^{-4} to 10^{-8} on a 96-well plate. Data are shown as mean \pm SEM. P-values represent statistical difference between polythiophene-treated and non-treated RML homogenates and were calculated with a Mantel-Haenszel Chi-square test (supplemental Table S1). Detection limit: Theoretical infectivity based on the observation of false positives at concentrations between 10^{-2} and 10^{-3} of non-infectious inoculum (mock). ***: $p < 0.001$, **: $p < 0.01$, *: $p < 0.05$. n/a: no positive wells were observed with this sample between concentrations ranging from 10^{-3} to 10^{-8} . ns: non significant $p > 0.05$. *D*, MPA assay was used to quantify prion aggregates in RML6 brain homogenates treated with increasing concentrations of PTAA, POMT, pHTAA or pFTAA. Each sample was analyzed in technical quadruplicates (circles) and is represented as the mean \pm SD. All data were corrected for the negative control (mock: CD1 brain homogenate) and represented as relative light units normalized for RML6 prions. Statistical differences were computed to compare LCP-treated RML6 to the control (non-treated RML6) (supplemental Table S1) or groups of four concentrations of each polythiophene (supplemental Table S6).

FIGURE 3. PTAA-treated RML6 prions are more sensitive to denaturation with GdnHCl. *A*, Immunoblots of non-treated (upper panels) and PTAA-treated RML6 brain homogenates at different concentrations of GdnHCl. RML6 brain homogenate was treated with either 10 µg ml⁻¹ (middle panel) or 100 µg ml⁻¹ PTAA (lower panel). Aliquots of 20 µg protein were denatured with various concentrations of GdnHCl, subsequently digested with PK to remove soluble PrP and loaded to the gel. The anti-PrP antibody POM1 was used for the detection. Molecular sizes are indicated in kDa. *B*, MPA of non-treated (open circles) and PTAA-treated RML6 brain homogenate (filled circles) after denaturation with different concentrations of GdnHCl. PTAA was used at a concentration of 10 µg ml⁻¹. Each sample was analyzed in technical duplicates and is represented as the mean \pm SD. All data were corrected for the negative control (CD1 brain homogenate) and represented as relative light units normalized for RML6 prions. Asymptotic curves were fitted to each dataset with the [GdnHCl]_½ value at which 50% of the molecules are in a soluble fraction and 50% are in an insoluble fraction indicated by a dotted line at 1.72 M for the non-treated and 0.31 M for the PTAA-treated samples.

FIGURE 4. PTAA affects prion replication, accumulation and neurodegeneration in slice cultures. *A*, Immunoblot from prion-infected slice cultures obtained from tga20 mice treated with different concentrations of PTAA. Cultures were harvested after 21 or 42 DIV and 20 µg total protein from all samples was digested with PK. The anti-PrP antibody POM1 was used for detection. Molecular sizes are indicated in kDa. The experiment was performed in biological triplicates and the immunoblot shown here is representative for the individual experiments. *B*, SCEPA of non-infected (mock) and RML6-infected slice cultures after exposure to PTAA. Infectivity of non-infected cultures harvested after 21 or 42 DIV are shown for comparison. PPS was used as a positive control. Each diamond represents the TCI₅₀ g⁻¹ of one slice culture homogenate determined by serial tenfold dilutions from 10^{-4} to 10^{-8} on a 96-well plate.

Error bars indicate the mean \pm SEM of biological triplicates. P-values represent the statistical differences between PTAA-treated and non-treated homogenates from RML6-infected slice cultures and are shown in supplemental Table S7. ***: $p < 0.001$, **: $p < 0.01$, *: $p < 0.05$. Detection limit (dashed line): Theoretical titer based on the observation of false positives at concentrations between 10^{-2} and 10^{-3} of non-infectious inoculum (CD1). n.s.: non significant. n/a: these results were not included into the statistical analysis. Because of mathematical complexity a statistical analysis could not be performed for slice cultures treated with $0.01 \mu\text{g ml}^{-1}$ PTAA. *C*, MPA of the slice culture homogenates shown in (A). Each dot represents the average value of technical triplicates for one slice culture homogenate. Error bars represent the mean \pm SEM of biological triplicates. All data were corrected for the negative control (mock) and represented as relative light units (RLU). P-values represent the statistical differences between PTAA-treated and non-treated homogenates from RML6 slice cultures and are shown in supplemental Table S8. ***: $p < 0.001$. *D and E*, Sandwich ELISA of the same homogenates as in (A) analysed for PrP^{Sc} (D) and PrP^C (E). Each dot represents the average value of technical duplicates for one slice culture homogenate. Error bars represent the mean \pm SEM of biological triplicates. All data were normalized to protein concentration of the corresponding sample. P-values are shown in supplemental Table S8. The ELISA was developed with a colorimetric substrate. The detection limit of 400 pg ml^{-1} (dashed line) was determined as the average background levels plus three times SD. *F*, Correlation diagram to show the relationship between the MPA and SCEPA data presented in (B) and (C). *G*, Correlation diagram to show the relationship between the SCEPA and ELISA data presented in (B) and (D). *H*, Correlation diagram to show the relationship between the MPA and ELISA data presented in (C) and (D).

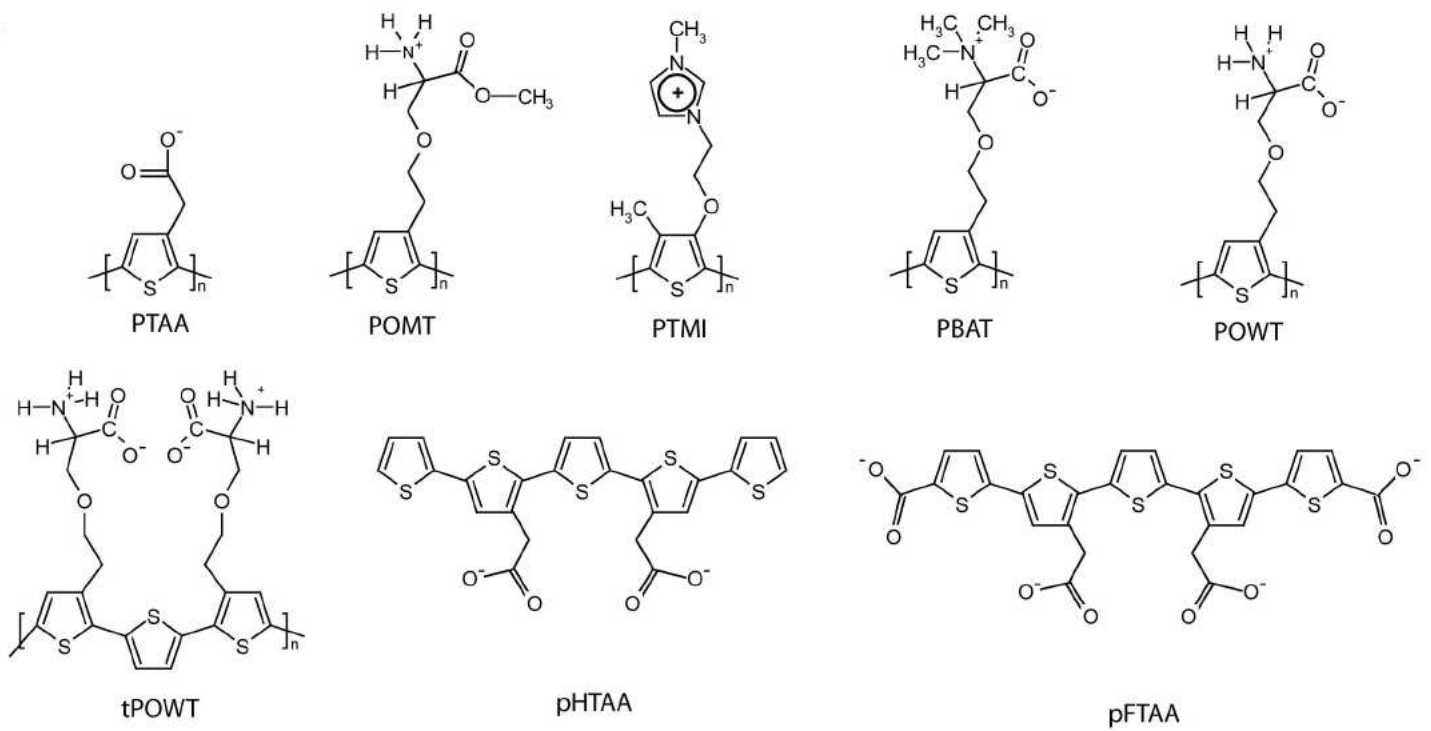
FIGURE 5. PTAA inhibits prion accumulation in RML6-infected slice cultures from different time points. *A*, MPA of homogenates from RML6 infected slices harvested at days 7, 19, 21, 28, 35 and 42 DIV. PTAA was administered at a concentration of $10 \mu\text{g ml}^{-1}$ at the time of medium change freshly into the medium from days 7, 19, 21, 28 or 35 DIV. Slice cultures were harvested at 42 DIV and analyzed for PrP aggregates. Each dot represents the average value of technical triplicates for one slice culture homogenate. Error bars represent the mean \pm SEM of biological duplicates. All data were corrected for non-infectious brain homogenates obtained from CD1 mice as negative control (mock) and represented as the ratio between relative light units (RLU) and protein concentration for each sample. P-values are shown in supplemental Table S9. *B*, Sandwich ELISA of the same homogenates as in (A) analysed for PrP^{Sc}. The data are represented as biological triplicates. The signal for the negative control (mock) is shown as single replica. *C*, Sandwich ELISA of the same homogenates as in (A) analysed for PrP^C. The ELISA was developed by chemiluminescence. The detection limit of 600 pg ml^{-1} (dashed line) was determined as the mean background levels plus three times SD.

FIGURE 6. Effect of PTAA on mPrP₂₃₋₂₃₁ fiber formation and preformed fibers. *A*, Time course of mPrP₂₃₋₂₃₁ fiber formation grown in the absence (filled circles) and presence of PTAA at different concentrations of $5 \mu\text{g ml}^{-1}$ (open circles), $10 \mu\text{g ml}^{-1}$ (filled squares), $25 \mu\text{g ml}^{-1}$ (open squares) and $50 \mu\text{g ml}^{-1}$ (filled diamonds) monitored by measuring the OD₃₅₀ over a period of 48h. Error bars represent the SD of technical triplicate measurements. *B*, TEMs taken after 48h of control fibers grown in the absence of PTAA and in the presence of different concentrations of PTAA. *C*, TEM of preformed mPrP₂₃₋₂₃₁ fibers incubated with different concentrations of PTAA. The electron micrograph in the right lower corner displays fibers incubated with $1 \mu\text{g ml}^{-1}$ PTAA at higher magnification. *D*, TEM of fibers recorded from another independent experiment grown in the presence of $10 \mu\text{g ml}^{-1}$ PTAA (upper panel) and of preformed mPrP₂₃₋₂₃₁ fibrils mixed with $1 \mu\text{g ml}^{-1}$ PTAA (lower panel). *E*, PTAA formed two different populations of small aggregates at concentrations between 1 and $10 \mu\text{g ml}^{-1}$ which were associated at the fibers with mean diameters of $43.9 \pm 6.1 \text{ nm}$ for population 1 (P1) and $16.8 \pm 2.5 \text{ nm}$ for population 2

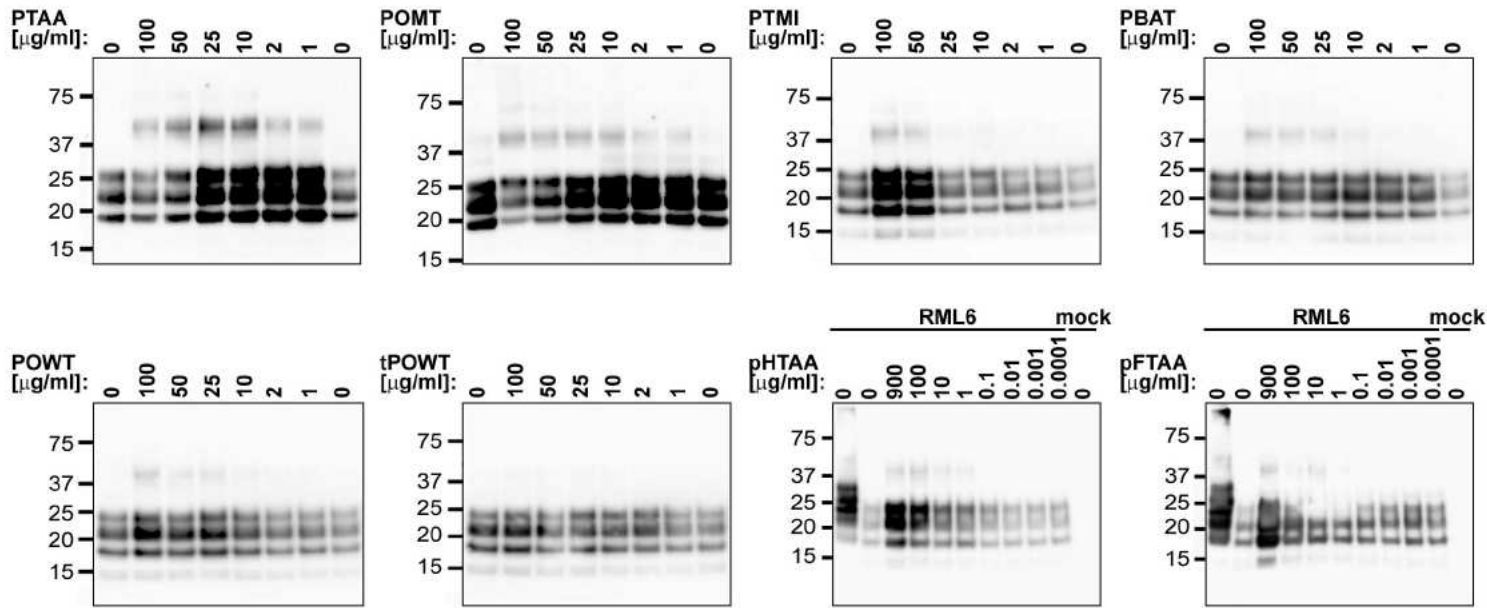
(P2). Free aggregates had mean diameters of 25.6 ± 7.4 nm for population 1 (FP1) and 15.4 ± 2.7 nm for population 2 (FP2). Data are represented as the mean \pm SD. *F*, PTAA aggregates were located on the fibers in a highly periodic manner with distances of 42.2 ± 12.5 nm for population 1 and 36.3 ± 8.6 nm for population 2. Data are represented as the mean \pm SD. *G*, PTAA increases the resistance of mPrP₂₃₋₂₃₁ fibers to PK digestion. Aliquots of mPrP₂₃₋₂₃₁ fibers were incubated with $10 \mu\text{g ml}^{-1}$ PTAA prior to proteolysis with increasing concentrations of PK. Lane 1 contains non-digested mPrP₂₃₋₂₃₁ fibers. Scale bar: 100 nm.

FIGURE 7. Model for the antiprion activity of the LCPs. *A*, In the prion model PrP^C is in a reversible thermodynamic equilibrium with PrP*, which further aggregates into amyloid fibrils, PrP^{Sc}. When the fibrils reach a critical length, the fibril becomes more fragile and fragmentation occurs. The newly formed ends of the fibril fragments are new nucleation sites for further fibril growth. *B*, The antiprion activity of the LCPs seems to be based on interactions with PrP^{Sc} aggregates, possibly increasing their compactness. LCP coated fibrils further embed preexisting prions and even PrP^C. The higher compactness of the PTAA treated aggregates ultimately cause less fragmentation into infectious particles necessary for further prion replication.

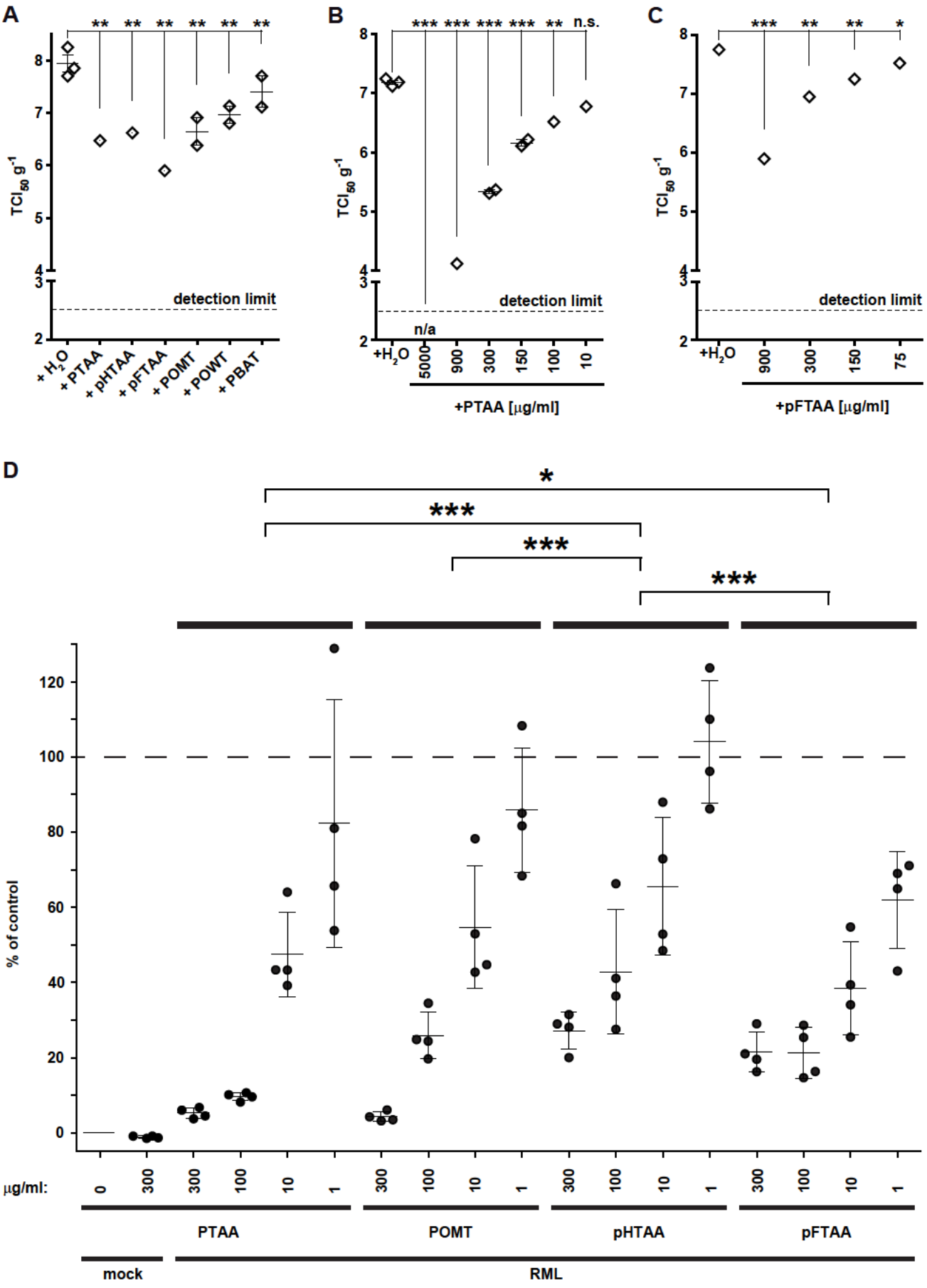
A



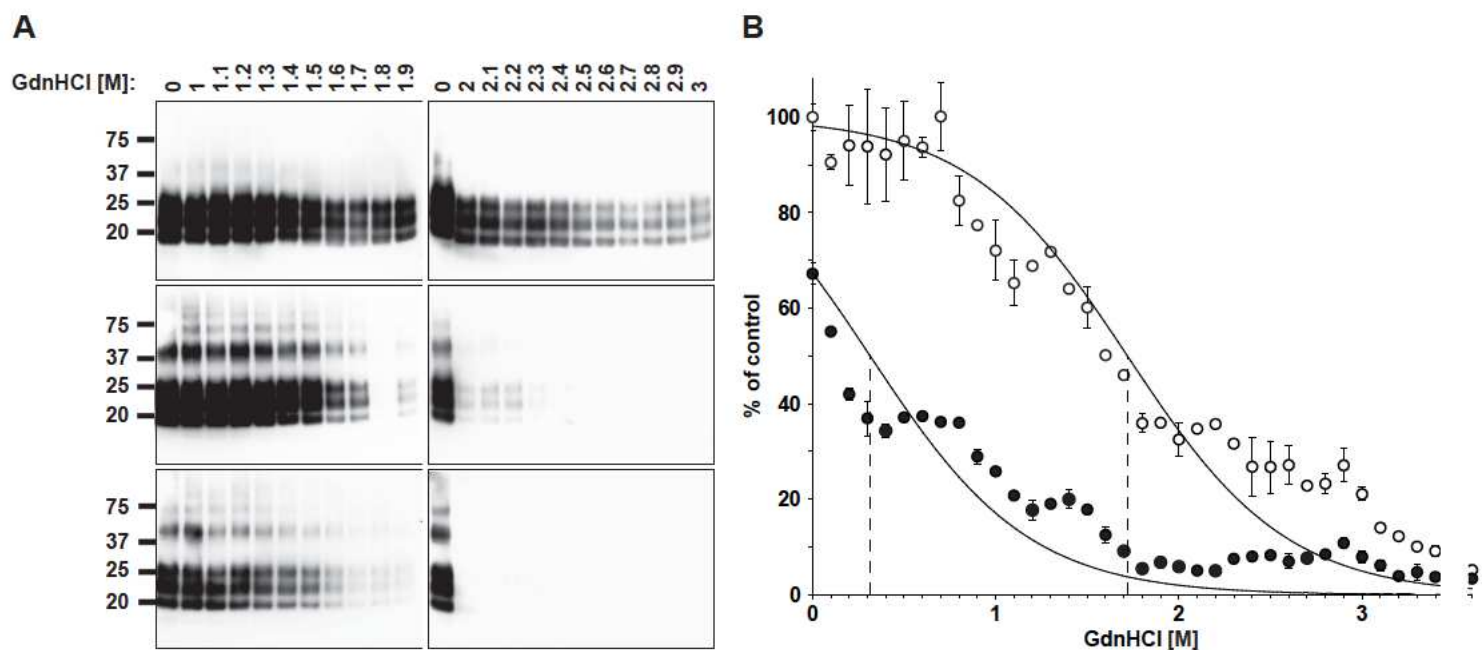
B

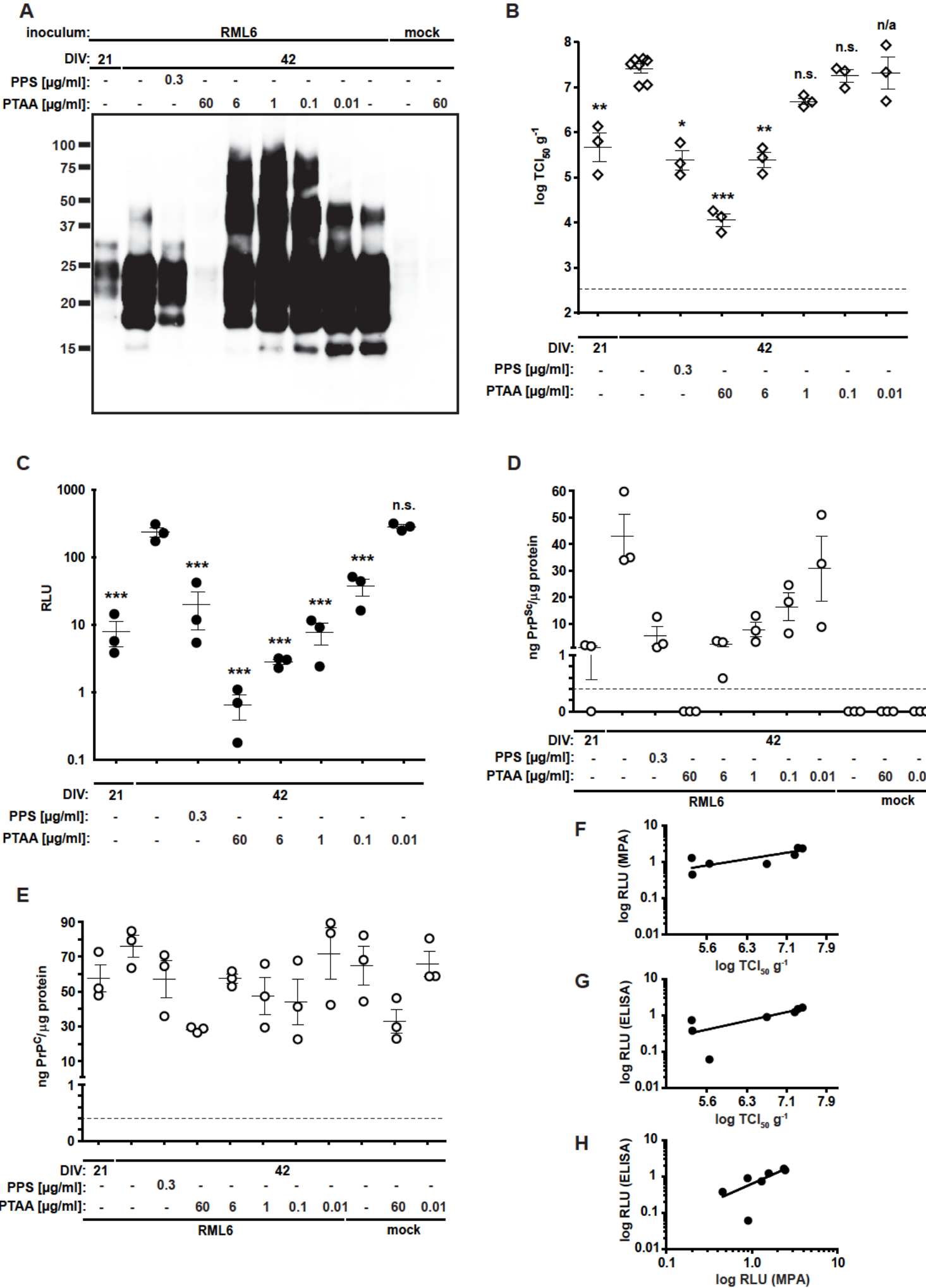


Margalith et al. Fig. 2

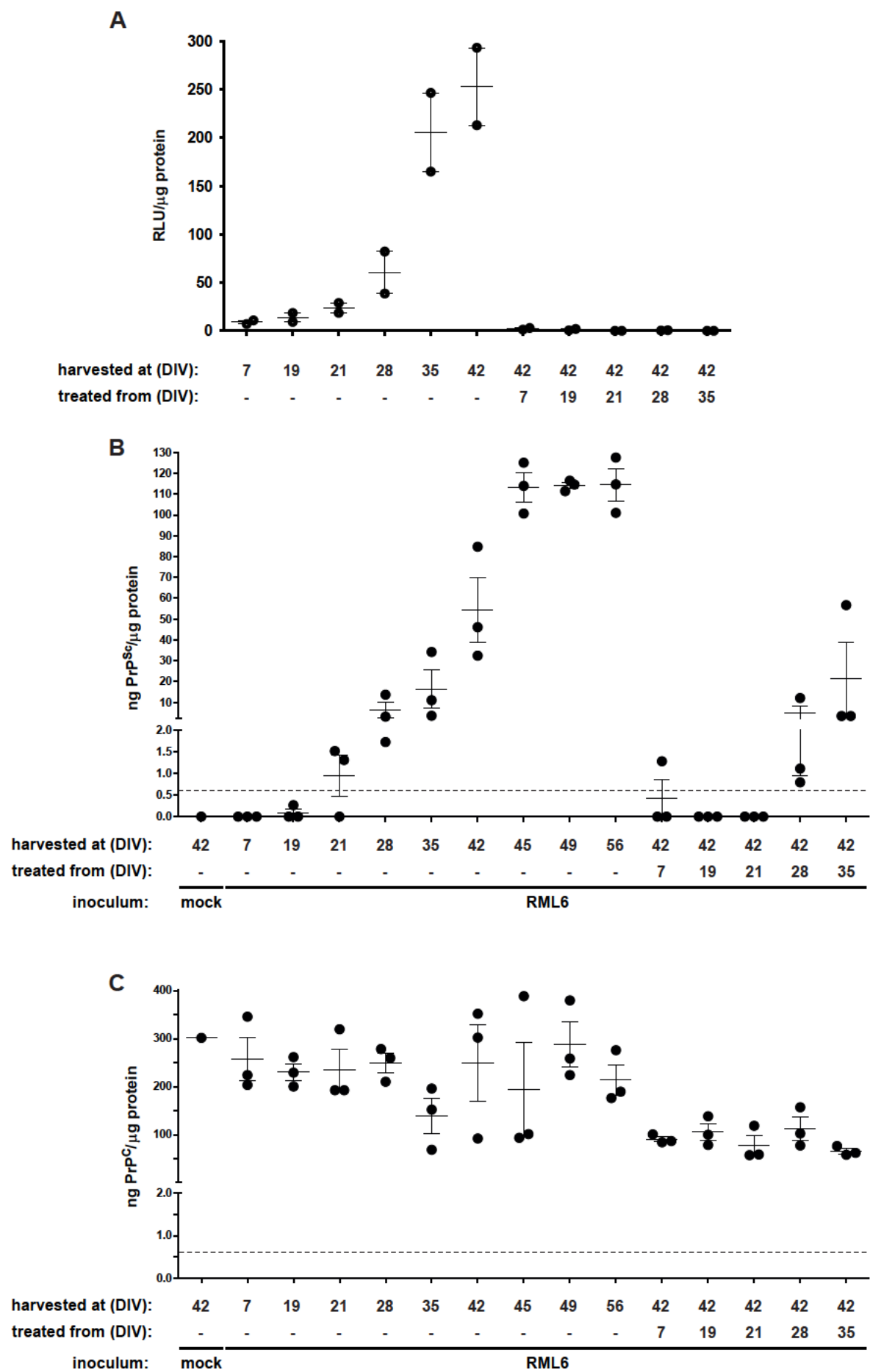


Margalith et al. Fig. 3





Margalith et al. Fig. 5



Margalith et al. Fig. 6

